Article

Evaluation of the Performance of Multi-Source Satellite Products in Simulating Observed Precipitation over the Tensift Basin in Morocco

Wiam Salih, Abdelghani Chehbouni and Terence Epule Epule *

International Water Research Institute (IWRI), Mohammed VI Polytechnic University (UM6P), Lot 660, Hay Moulay Rachid, Benguerir 43150, Morocco; wiam.salih@um6p.ma (W.S.); abdelghani.chehbouni@um6p.ma (A.C.)
* Correspondence: epule.terence@um6p.ma

Abstract: The Tensift basin in Morocco is prominent for its ecological and hydrological diversity. This is marked by rivers flowing into areas such as Ourika. In addition to agriculture, the basin is a hub of variable land use systems. As such, it is important to gain a better understanding of the relationship between simulated and observed precipitation in this region to be able to better understand the role of precipitation in impacting the climate and water resources in the basin. This study evaluates the performance of multi-source satellite products against weather station precipitation in the basin. The satellite-product-based data were first collected for seven satellite products, namely PERSIANN, PERSIANN CDR, TRMM3B42, ARC2, RFE2, CHIRPS, and ERA5 (simulated precipitation) from the following repositories (CHRS iRain, RainSphere, NASA, EUMETSAT, NOAA, FEWS NET, ECMWF). Precipitation observation data from six weather stations, located at Tachedert (2343 m), Imskerbour (1404 m), Asni (1170 m), Grawa (550 m), Agdal (489 m), and Agafay (487 m), at different altitudes, latitudes, and temporal scales (1D, 1M, 1Y), over the period 13 May 2007 and 31 September 2019 over the Tensift basin were collected. The data were compared and analyzed through inferential statistics such as the Nash–Sutcliffe efficiency coefficient, bias, root-mean-square error (RMSE), root-mean-square deviation (RMSD), the standard deviation, the correlation coefficient (R), and the coefficient of determination (R^2) and visualized through Taylor diagrams and scatterplots to visualize the closeness between the seven satellite products and the observed precipitation data. A second analysis was carried out on the monthly precipitation, resulting from the six weather stations, and based on the standardized precipitation index (SPI) to determine the onset, duration, and magnitude of the meteorological drought. The results show that PERSIANN CDR performs best and is more reliable regarding its ability to simulate precipitation over the basin. This is seen as PERSIANN CDR has significant rates for the different statistics (Bias: −0.05 (Daily Asni), RMSE: 2.86 (Daily Agdal), R: 0.83, R^2:0.687 (Monthly Agdal)). The results also show that there are no major differences between the observed weather station and the satellite precipitation data. The best performance was attributed to PERSIANN CDR (for monthly and annual precipitation at all altitudes and for daily precipitation at high altitudes). However, most of the time, this product records low or negative Nash values (−6.06 (Annual Grawa)), due to the insufficient weather station data in the study area (Tensift). It was observed that TRMM overestimates precipitation during heavy precipitation and underestimates it during low precipitation. This makes it important for the latter observations to be viewed with caution due to the quality of annual comparison results and underscores the need to develop more efficient precipitation comparison approaches and datasets. Additionally, the performance of the satellite products is better at low altitudes and during wet years. Finally, it was concluded from the SPI that Tensift region has experienced 13 drought periods over the study period, with the longest event of 12 months being from Marsh 2015 to February 2016, and the most intense event with the highest drought severity (19.6) and the lowest SPI value (−2.66) being in 2019.

Keywords: precipitation; Tensift basin; remote sensing; spatiotemporal; satellite products; PERSIANN CDR; TRMM; weather stations; SPI

1. Introduction

Global change processes such as global warming and climate change are impacting the intensity and frequency of extreme weather events, droughts, floods, and consequently, the various phases of the hydrological cycle (IPCC Sixth Assessment Report: AR6) [1]. Africa is one of the most vulnerable continents to climate change and variability due to its high exposure and low adaptive capacity to climate change and variability. Since the Fourth Assessment Report (AR4), several studies have suggested that climate variability in Africa will have greater impacts on future water resources relative to other factors, such as population growth, urbanization, agricultural growth, and land use change [1]. Furthermore, the most recent IPCC report (AR6) notes that mean temperatures and hot extremes have increased in all regions of Africa, with projections showing that the rate of surface temperature in Africa will rise faster than the global land average, particularly in the more arid regions of Africa, including Morocco [1]. Based on multiple emissions scenarios, a global warming of 2 °C, relative to 1850–1900, would be exceeded during the twenty-first century (Special Report on Emissions Scenarios: SRE) [1]. As a result, there are likely to be less frequent and more intense and heavy precipitation events with projected decreases in mean precipitation across Africa [1]. This will likely lead to increase in agricultural and ecological droughts [1]. In North Africa, both minimum and maximum mean annual temperatures are likely to increase, with a strong decrease in precipitation under the A1B and A2 scenarios [1]. This will significantly affect countries in Northern Africa, such as Morocco, due to its huge dependence on winter precipitation, and would be negatively impacted if total precipitation and frequency of wet days declines.

Analysis of the CHIRPS satellite product over the Tensift basin by Habitou [2] show that the basin had experienced eight severe droughts during the last four decades, with the driest year being 2019 with droughts being a common phenomenon in the Tensift basin [2]. The availability of water is one of the most important variables impacting socio-economic development in semiarid and arid climate zones, mainly because such regions are largely dependent on agricultural incomes. Therefore, novel information on the spatial and temporal distribution of satellite-based and observed precipitation data are essential in enhancing understanding of the hydrological cycle, and the accuracy of its spatial and temporal distribution [3]. As a result, it is important to develop adequate monitoring options that are capable of monitoring and facilitating policy actions for better adaptation. In addition, improvements in the ability to measure and simulate hydro-meteorological events have become paramount because such data enhance readiness for adaptation to climate variability. This is especially relevant in the context of the most vulnerable regions of Africa, such as Morocco in general and Tensift in particular [3]. In recent decades, this phenomenon has gained grounds due to significant decrease in precipitation, irregular spatial and temporal precipitation distribution, and more intense and frequent drought events [4]. On the other hand, the ramifications of these global change processes have not only been limited to precipitation declines but have also been manifested in extreme precipitation events and floods. The recurrent flooding phenomenon is common in large metropolises that have experienced catastrophic floods in recent decades, causing considerable damage [5]. Therefore, understanding these extreme events is of great importance in the monitoring and developing of actions to enhance adaptation. Hence, it is paramount to have more studies that effectively measure and compare simulated and observed precipitation to better understand climate variability as well as improve the accuracy of climate policy and adaptations.

Although in situ measurement instruments or weather-station-based data (rain gauges, etc.) provide a partial solution to this issue at specific scales, they do not respond to the daunting question of monitoring variables both in space and in time. It is true that the most obvious solution in this case would be to expand the network of weather stations, an issue that is highly limited in Africa considering data availability and the cost related to establishing such infrastructure. Therefore, the feasibility of the latter is impacted by cost, maintainability, as well as accessibility to many areas [5]. As a result of the above limita-

tions, interest in remote sensing through satellite products is gaining in prominence. This alternative offers a robust and efficient solution to improve the spatiotemporal monitoring of precipitation over large areas, and thus provides great opportunities for researchers to better understand climate variability [6–8]. Therefore, this study assesses the ability of satellite products at different spatial scales (0.25° × 0.25°, 0.1° × 0.1°, 0.05° × 0.05°), altitudes (2343 m, 1404 m, 1170 m, 550 m, 489 m, 487 m) and temporal scales (24 h, 1 month, 1 year) in evaluating the performance of the different satellite products in simulating precipitation in the Tensift basin of Morocco.

This work compares the pixels of the different satellite grids (PERSIANN, PERSIANN CDR, TRMM3B42, ARC2, RFE2, CHIRPS, and ERA5) with the corresponding pixels of in situ precipitation data from six weather stations (Tachedert, Imskerbour, Asni, Grawa, Agdal, and Agafay) in the Tensift basin. To the best of our knowledge, at the time of writing this paper this work represented the first attempt at providing an evaluation and a comparison of these seven satellite precipitation products with the observations from six weather stations at three-time steps over the Tensift basin. This effort will help in creating a new compendium or a data platform from which a better understanding of the relationship between satellite-based precipitation data and weather station precipitation data can be established and studied. The uniqueness of this study is that there are currently no evaluations of several satellite precipitation data products in the Tensift basin. Insufficient in situ data required for statistical comparison are often major challenges in precipitation monitoring initiatives across Africa, as reported in AR4 [1,2]. As such, the use of satellite products is one good way of filling this gap and making such data available to the research community for further investigations. This is important because it will develop an integrated analysis and improve knowledge on climate variability. Additionally, there are no studies that have also explored the altitudinal and spatial dimensions of these dynamics within the Tensift basin.

2. Materials and Methods

2.1. Study Area

The Tensift watershed, located in the Marrakech–Safi region in central–western Morocco, covers 24,000 km^2 [2]. It is characterized by an arid climate that is governed by complex orography, as well as humid conditions due to its proximity to humid and cold air masses from the Atlantic Ocean [9]. This basin has a hydrological system that links rivers from upstream downstream. The high Atlas Mountains feed the Haouz of Marrakech (the plain) through the wadis (Tensift, Ourika, Chichaoua, and N'Fiss), the underground and deep flows [10]. These rivers are fed by rainfall, as well as by snowmelt from the mountains, which accounts for 25% of the flow [11]. The highest elevation of this region is about 4167 m (Jebel Toubkal); it receives an annual average precipitation of between 300 and 800 mm. On the other hand, the basin records an average precipitation of about 250 mm per year [2,10]. The Haouz has experienced a significant extension of irrigated areas in recent decades, which extend over 2000 km with a dominance of wheat cultivation (80%) followed by olive trees, citrus fruits, apricot trees, market gardening, vineyards, and fodder. This drives over-exploitation of the irrigation waters flowing from the surface streams and rivers [11]. For the location of the Tensift basin of Morocco, see Figure S1.

2.2. Data Collection

To be able to assess the performance of the seven satellite-based precipitation products in their ability to simulate observed weather-station-based precipitation in the Tensift basin of Morocco, this study resorted to collecting data from various sources, as shown below.

2.2.1. Weather Station Data

To facilitate the comparison of simulated precipitation (satellite) with observed precipitation (weather station), this study collected daily observed precipitation data, over the period 13 May 2007 and 31 September 2019, from six weather stations located in the Tensift

basin, provided by LMI_TREMA [11]. These stations included the Tachedert weather station (31,155, −7.847) located at an altitude of 2343 m, representing high-altitude precipitation data. The second set of weather stations were those which provided medium-altitude precipitation data such as Imeskerbour (31.204, −7.94), located at an altitude of 1404 m, and Asni (31.245, −7.984), located at an altitude of 1170 m. Finally, the weather stations representing low-altitude precipitation data in the Tensift region included weather stations such as Grawa (31.584, −7.916), Agdal (31.6, −7.981), and Agafay (31.5, −7.916), with altitudes of 550 m, 489 m, and 487 m, respectively. The locations of the weather stations in the region are presented in Figure S2 in the Supplementary Materials. These weather stations were selected based on the availability of data (Table S1).

The evaluation of the weather stations products was carried out over the period 13 May 2007 to 31 September 2019 (Table 1). The average, maximum, and standard deviation of the rainfall decreased with altitude, except for Agafay, which had the highest maximum value (97.4) after Tachedert, even though it was located at low altitude; similarly, for the average (0.85) and the standard deviation (4.06). However, Grawa had the lowest availability of the data (64.43%), in contrast to Tachedert, which had an availability of 96.3%. A second evaluation of the data was carried out by testing their homogeneity; the double mass test was established between the observed gauges. The results showed a homogeneity of the data and an average coefficient correlation of the cumulative rainfall of all stations of $R^2 = 0.987$. The data have been used in different studies over the Tensift basin, including research by Er-Raki [12], El Khalki [13], and Baba [14].

Table 1. Statistical criteria of weather station observations over the period 13 May 2007 to 31 September 2019.

	Tachedert	Imskerbour	Asni	Grawa	Agafay	Agdal
Min	0	0	0	0	0	0
Max	244.2	71.2	64.6	63.4	97.4	61.3
Mean	1.53	1.12	0.84	0.53	0.85	0.55
Standard Deviation	6.97	4.26	3.87	2.76	4.06	2.57
Availability of Data	96.3%	96.04%	87.22%	64.43%	95.32%	94.8%

2.2.2. Satellite and Reanalysis Data

In the context of the satellite-based products, data for seven key products were collected over the period 13 May 2007 to 31 September 2019. The collection was based on the availability of the data for the Tensift basin (Tables S1 and S2). Unfortunately, data are currently not available beyond these dates for all seven products for the Tensift basin. Below is a description of the characteristics of these satellite products and their sources.

Precipitation Estimation from Remotely Sensed Information using Artificial Neural Networks (PERSIANN)

The PERSIANN precipitation products were developed by the Center for Hydrometeorology and Remote Sensing (CHRS) at the University of California, Irvine, in collaboration with NASA, NOAA, and UNESCO's Global Network for Water and Arid Lands Development Information (G-WADI) program. They use artificial neural network (ANN) models to estimate precipitation from cloud-top temperatures measured using the infrared (IR) spectrum range (10.2–11.2 μm). The latter also uses geostationary satellite imagery from GOES-8, GOES-9/10, GOES-12, GMS-5, METEOSAT-6, and METEOSAT-7, provided by NOAA, and incorporates passive microwave imagery from low Earth orbiting (LEO) satellites to continuously update the model parameters. Sometimes, this model can even use other high-quality precipitation estimates, such as weather stations and radars, to improve the forecast. The output data have a spatial resolution of 0.25° × 0.25° and temporal

resolutions of 3, 6, and 24 h. The geographical area covered by the algorithm extends from latitude 50°N to 50°S, and the product has been available since March 2nd, 2000 [8]. The PERSIANN family includes three satellite precipitation estimation products, namely, PERSIANN, PERSIANN CCS, and PERSIANN CDR, which were collected from the following databases: CHRS iRain [15] (http://irain.eng.uci.edu: accessed on 15 July 2021), Data Portal [16] (http://chrsdata.eng.uci.edu: accessed on 15 July 2021), and Rain Sphere [17] (http://rainsphere.eng.uci.edu: accessed on 15 July 2021). However, for this study, only PERSIANN and PERSIANN CDR were used.

Precipitation Estimation from Remotely Sensed Information using Artificial Neural Networks—Climate Data Record (PERSIANN CDR)

PERSIANN CDR has used a modified PERSIANN algorithm to produce precipitation estimates since 1983. This product uses infrared imagery data from GridSat-B1, which have been available since 1979 at a spatial resolution of 10 km and a temporal resolution of 3 h, instead of passive microwave imagery (MOP), to train the nonlinear regression parameters of the ANN model. Then, the data are adjusted for 3-hourly rainfall estimates by incorporating information from the Global Precipitation Climatology Project (GPCP) every 2.5 months. Thus, it provides daily precipitation estimates with a spatial resolution of $0.25° \times 0.25°$ for the latitudinal band 60N–60S, available since 1 January 1983 [18].

Tropical Rainfall Measuring Mission (TRMM)

The TRMM-3B42 algorithm is an estimation of precipitation product developed by NASA. It combines satellite- and ground-based data. First, the GNU profiler (GPROF) algorithm integrates MOP data from the LEO TRMM/TMI, AQUA/AMSR-E, DMSP/SSMI, and AMSU-B satellites as a first precipitation estimate. These estimates are then calibrated based on TRMM/TMI Combined Instrument (TCI) data and adapted to a $0.25° \times 0.25°$ resolution grid. Moreover, these calibrated products are merged with IR data from the GOESW, GOES-E, GMS, METEOSAT-5 and METEOSAT-7, and NOAA-12 satellites. Finally, a correction is made using Global Precipitation Climatology Centre (GPCC) ground data. The output of the TRMM3B42 (v) algorithm has a temporal resolution of 3 h with rainfall rate values in mm h^{-1}. The geographical area covered extends from latitude 50°N to 50°S for a spatial resolution grid of $0.25° \times 0.25°$ [8,16–22]. The product data have been available since 1 January 1998, to 31 December 2019, and were accessed from [23] (https://earthdata.nasa.gov/: accessed on 15 July 2021).

African Rainfall Climatology Version 2 (ARC2)

The ARC2 product was developed by the Climate Prediction Center (CPC), and it is a precipitation estimate algorithm derived from the combination of European Organization for the Exploitation of Meteorological Satellites (EUMETSAT) 3-hourly IR data centered over Africa, and the Global Telecommunications System (GTS) 24-hourly weather station measurements. The estimated precipitation (mm/h) from this algorithm covers the whole of Africa and has a spatial resolution of $0.25° \times 0.25°$ and a temporal resolution of 24 h [24]. These data have been available since 1 January 1983 and were accessed from [25] (https://iri.columbia.edu/: accessed on 30 July 2021).

Rainfall Estimation Algorithm Version 2 (RFE2)

RFE2 is an estimation product that was developed by the NOAA Climate Prediction Center. It is an estimation technique based on the fusion of 4 data sources, namely, daily GTS weather station data (1000 stations), estimation of satellite MOP AMSU (4 times a day), satellite SSM/I (4 times a day), and finally, the precipitation GPI estimated from cloud-top infrared temperature every half an hour. These satellite estimates are first linearly combined using predetermined weighting coefficients and then merged with the GTS data to determine the final precipitation over Africa. The output files have a spatial resolution of 0.1° and temporal resolution of 24 h, and a spatial extent of 40°S–40°N

and 20°W–55°E. They have been available since 2002 and were accessed from [26] (http://www.cpc.ncep.noaa.gov/products/GIS/GIS_DATA/: accessed on 30 July 2021).

The Climate Hazards Group Infrared Precipitation with Stations (CHIRPS)

　　CHIRPS is a new quasi-global (50°S–50°N) daily and monthly precipitation estimation product with high resolution (0.05°). It was developed by experts from the U.S. Geological Survey Earth Resources Observation and Science Center in collaboration with the Climate Hazards Group at the University of Santa Barbara, California [2]. It was developed to support the United States Agency for International Development Famine Early Warning Systems Network (FEWS NET). It uses both infrared data and Tropical Precipitation Measurements Version 7 (TMPA 3B42 v7) to calibrate the cold cloud duration (CCD) precipitation estimates. CHIRPS integrates the weather station data in two phases, thus producing two unique products. The first phase produces a preliminary product with a latency of 2 days, combining the GTS rain gauge data with the CCD precipitation estimates. The second phase gives the final product with a latency of 3 weeks; the monthly weather station data are combined with the monthly CCD estimates to produce fields such as the GPCC products [27]. They have been available since January 1981 and were accessed from [28] (https://edcintl.cr.usgs.gov/downloads/sciweb1/shared/fews/web/global/monthly/chirps/final/downloa ds/monthly/: accessed on 30 July 2021).

ECMWF Reanalysis 5th Generation (ERA5)

　　ERA5 is an atmospheric reanalysis product developed by the European Centre for Medium-Range Weather Forecasts (ECMWF). Large-scale precipitation is generated from the cloud scheme, whereas convective precipitation is retrieved from the convective scheme [26,27,29,30]. For this study, an hourly ERA5 (0.25° × 0.25°) reanalysis dataset covering the Tensift region over the period from January 1980 to June 2020 was imported from the interface [31] (https://cds.climate.copernicus.eu/#!/home: accessed accessed on 30 July 2021).

2.3. Data Analysis

　　In this study, a comparison between three weather station datasets over the Tensift basin (Tachedert, Asni, and Grawa) and the corresponding pixel of each satellite product (PERSIANN, PERSIANN CDR, TRMM3B42, ARC2, RFE2, CHIRPS, and ERA5) was performed at different altitudes and spatiotemporal scales (daily, monthly, and annual). To understand the relationship between the different satellite products and weather station observations, as well as characterize and analyze the biases and errors, the following empirical tests were used: Nash–Sutcliffe (NASH), bias correction (BC), the root-mean-square error (RMSE), the correlation coefficient (R), and the coefficient of determination (R^2). A detail description of these empirical approaches and the equations used are presented below.

2.3.1. NASH (Nash–Sutcliffe)

　　The Nash–Sutcliffe criterion is a performance indicator with values in the interval (1 to $-\infty$ infinity). It is used to estimate the ability of a model to reproduce an observed behavior. The closer the value obtained by this criterion is to 1, the closer the simulated values (satellite products) are to the observed values (weather station data). It is generally accepted that the Nash–Sutcliffe criterion must be greater than 0.7 to be able to state that a model is satisfactory and the estimated and observed values are consistent. If the Nash–Sutcliffe criterion is equal to 0, it means that the model does not perform well in simulating the output with the average of the observed values. When the criterion becomes negative, it indicates an even less predictive model [8]. The equation used to fit this empirical model is given below (Equation (1)).

$$Nash = 1 - \frac{\sum_{i=1}^{n}(X_{obs\ i} - X_{sim\ i})^2}{\sum_{i=1}^{n}(X_{obs\ i} - \overline{X_{obs}})^2} \tag{1}$$

where n represents the number of observations, $X_{obs\ i}$ stands for the ith observed value at the weather stations, $X_{sim\ i}$ is the ith simulated value by the satellite, and $\overline{X_{obs}}$ is the average of the observed values.

2.3.2. Bias

The bias represents the difference between the averages of the satellite estimates and those of the weather station. This method makes it possible to predict whether the satellite products overestimate or underestimate precipitation rates on average. For the satellite products to be validated, the bias must be as close to zero as possible [8]. The equation used to fit the bias is given below (Equation (2)).

$$\text{Bias} = \frac{1}{n}\sum_{i=1}^{n}(X_{sim\ i} - X_{obs\ i}) = \frac{1}{n}\sum_{i=1}^{n}\in_i \tag{2}$$

where n represents the number of observations, $X_{obs\ i}$ is the ith observed value at the weather station, $X_{sim\ i}$ is the ith simulated value by the satellite, and $\in_i$ is the difference between each observation i and the estimate i.

2.3.3. Root-Mean-Square Error (RMSE)

The root-mean square error (RMSE) measures the average magnitude of the error. The values of RMSE are always positive and are found in the interval $(0; +\infty$ infinity). Contrary to the bias, which indicates the error without information on the magnitude, the RMSE criterion gives an idea about this amplitude. Thus, a model judged to be accurate by the bias (close to zero) may still be very inaccurate (high RMSE values) due to the compensation between the positive and negative values. Therefore, the accuracy of the model can only be judged if the RMSE value is close to zero. Nevertheless, this indicator does not show the over- or underestimation of the model compared with the observations. Therefore, the bias is complementary to the RMSE [8]. The equation used to compute the RMSE is given below (Equation (3)).

$$\text{RMSE} = \sqrt{\frac{1}{n}\sum_{i=1}^{n}(\in_i)^2} \tag{3}$$

where n represents the number of observations, and $\in_i$ is the difference between each observation i and estimate i.

2.3.4. Root-Mean-Square Deviation (RMSD)

The RMSD is used to measure the differences between the values predicted by a model or estimator and the observed values. The RMSD is the square root of the second sampling moment of the differences between the predicted and observed values. The RMSD is always positive, and a value of 0 would indicate a perfect fit to the data. In general, a smaller RMSD value indicates better accuracy than a higher RMSD value [8]. The equation used to fit the RMSD is given below (Equation (4)).

$$\text{RMSD} = \sqrt{\frac{1}{n}\sum_{i=1}^{n}\left(\left(X_{sim\ i} - \overline{X_{sim}}\right) - \left(X_{obs\ i} - \overline{X_{obs}}\right)\right)^2} \tag{4}$$

where n represents the number of observations, $X_{sim\ i}$ is the ith simulated value by the satellite, $\overline{X_{sim}}$ is the average of the simulated values, $X_{obs\ i}$ stands for the ith observed value by the weather station, and $\overline{X_{obs}}$ is the average of the observed values.

2.3.5. Standard Deviation

The standard deviation is a measurement of the degree of variation or dispersion of a set of values. A low standard deviation implies that the values are close to the mean,

whereas a high standard deviation shows that the values are spread out over a larger range [8]. The equation used to fit the standard deviation is given below (Equation (5)).

$$S = \sqrt{\frac{1}{n} \sum_{i=1}^{n} ((X_i - \overline{X})^2}$$

(5)

where *n* stands for the shape of the set, X_i is the *i*th value, and $\overline{X}$ is the average of the set.

2.3.6. Correlation Coefficient (R)

The correlation coefficient is a measure which quantifies the strength of a linear relationship between two variables. The approach compares the distance of each data point from the mean of the variable and uses it to indicate to what extent the variable relationship follows an imaginary line. The correlation coefficient R is a no unit value between −1 and 1. Positive values of R indicate a positive correlation, i.e., the values of the two variables tend to increase together. Negative values of R indicate a negative correlation, i.e., the values of one variable tend to increase and the values of the other variable decrease. The values 1 and −1 each represent "perfect" correlations, positive and negative, respectively. Two variables with a perfect correlation move together at a fixed rate [8]. The equation used to fit the R is given below (Equation (6)).

$$R = \frac{\sum \left[\left(X_{obs\ i} - \overline{X_{obs}} \right) \left(X_{sim\ i} - \overline{X_{sim}} \right) \right]}{\sqrt{\sum (X_{obs\ i} - \overline{X_{obs}})2 * (X_{sim\ i} - \overline{X_{sim}})2}}$$

(6)

where $X_{sim\ i}$ is the *i*th simulated value by the satellite, $\overline{X_{sim}}$ is the average of the simulated values, $X_{obs\ i}$ stands for the *i*th observed value at the weather station, and $\overline{X_{obs}}$ is the average of the observed values.

2.3.7. Coefficient of Determination (R^2)

The coefficient of determination R^2 is the square of the correlation coefficient. It judges the quality of the linear regression. It ranges between 0 and 1 and measures the adequacy between the estimated and observed data. The closer the coefficient of determination is to 0, the more the scatterplot spreads around the regression line. In contrast, the closer the R^2 is to 1, the tighter the scatterplot is around the regression line. When the points are exactly aligned on the regression line, $R^2 = 1$ [8]. The equation used to fit the R^2 is given below (Equation (7)).

$$R = \left(\frac{\sum \left[\left(X_{obs\ i} - \overline{X_{obs}} \right) \left(X_{sim\ i} - \overline{X_{sim}} \right) \right]}{\sqrt{\sum (X_{obs\ i} - \overline{X_{obs}})^2 * (X_{sim\ i} - \overline{X_{sim}})^2}} \right) 2$$

(7)

where $X_{sim\ i}$ is the *i*th simulated value by the satellite, $\overline{X_{sim}}$ is the average of the simulated values, $X_{obs\ i}$ stand for the *i*th observed value at the weather station, and $\overline{X_{obs}}$ is the average of the observed values.

2.3.8. Standardized Precipitation Index (SPI)

Thomas B. McKee created the SPI as a tool for describing drought events. It is a measure which is based on precipitation data and may be used to examine wet and dry periods. The SPI compares precipitation at a given time (typically 1 to 24 months) annual precipitation, mean precipitation, and the standard deviation. Table S3 shows a classification system for determining the severity of drought occurrences based on the SPI value [3]. SPI involves normalized, standardized precipitation values; therefore, the threshold SPI for specific classes corresponds to the definite probabilities of non-exceeding a given value of standardized precipitation. The equation used to fit the SPI is given below (Equation (8)).

$$SPI = f(p) - u/SD$$

(8)

where SPI is the Standardized Precipitation Index, *f(p)* is the transformed sum of precipitation, *U* is the mean value of the normalized precipitation, *SD* is the standard deviation of the normalized precipitation sequence.

3. Results

3.1. Annual Cumulative Satellite-Based Average and Cumulative Rainfall

The results of this work have shown that the average annual precipitation of the data availability period (13 May 2007 to 31 December 2019) tilts towards a strong gradient of precipitation between the north and south of the country as precipitation declines southwards. The mean annual rainfall in Morocco decreases from the north to the south as well as from the west to the east, and ranges from more than 500 mm in the northern part, to between 250 mm and 400 mm in the central region, and between 150 mm and 250 mm in the southern region (south of the high Atlas), and less than 100 mm in the Sahara Desert. There are also very important disparities between the various satellite products, as the maximum average annual precipitation varies from 250 mm for TRMM to 1000 mm for CHIRPS (Figure 1). It can be observed that the cumulative precipitation of the wettest year (2010) detected by CHIRPS was (2000 mm), ARC2 was (1600 mm), CDR was (1000 mm), and higher than the values detected by PERSIANN (500 mm) and TRMM (400 mm) (Figure 2). Indeed, the better performance of PERSIANN CDR over PERSIANN can be explained by the bias adjustment of PERSIANN CDR on a monthly scale using GPCP data. Furthermore, the cumulative precipitation rates of the driest year of the study period (2019) maintains the same order as the previous figures with a better performance recorded for the CHIRPS product (900 mm) and a relatively worse performance of TRMM (350 mm) and PERSIANN (250 mm) products. For this dry year (Figure 3), it can be observed that the gaps between the products have decreased and the performance of TRMM has improved compared with 2010 (Figure 2).
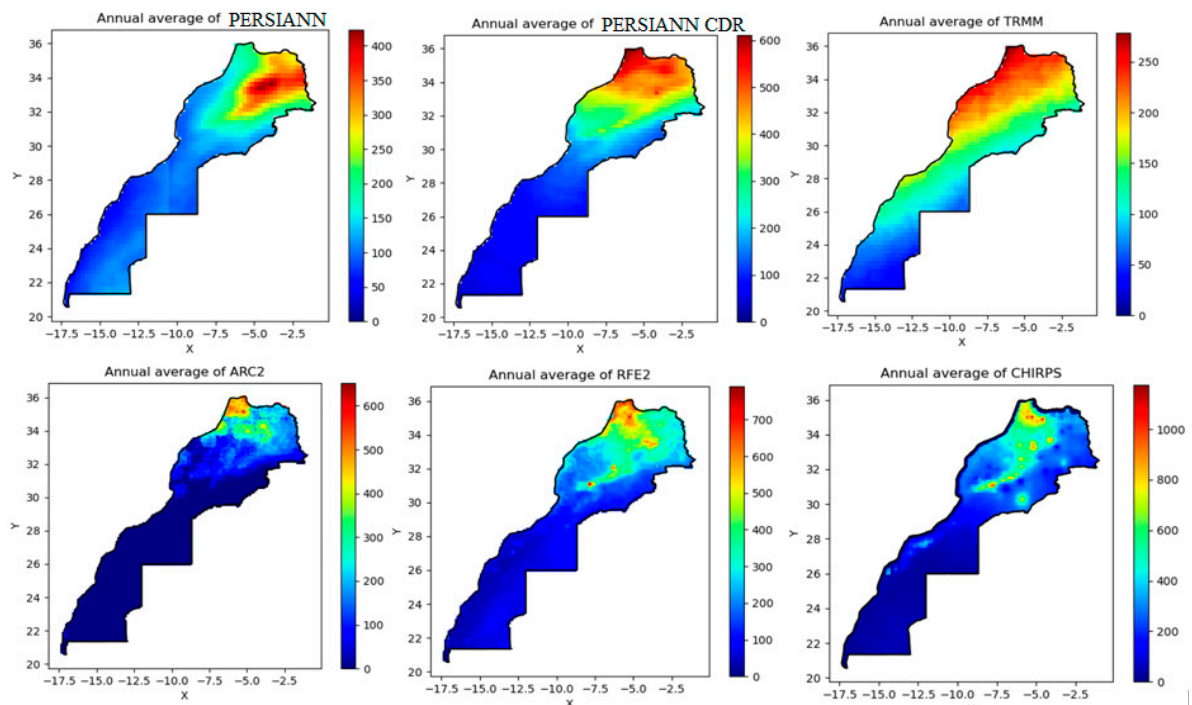
Figure 1. Simulated satellite-based average annual rainfall for the study period. (x: longitude, y: latitude).
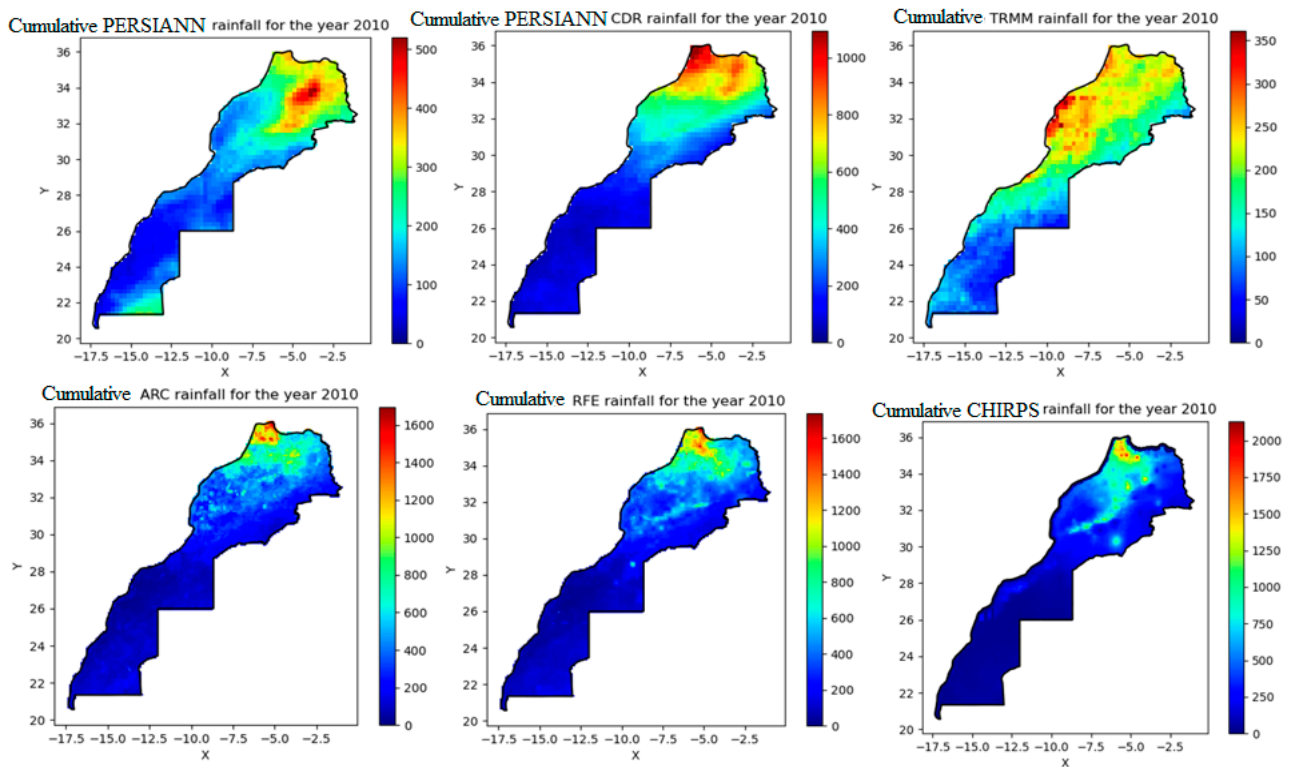
Figure 2. Simulated satellite-based cumulative rainfall for the year 2010.
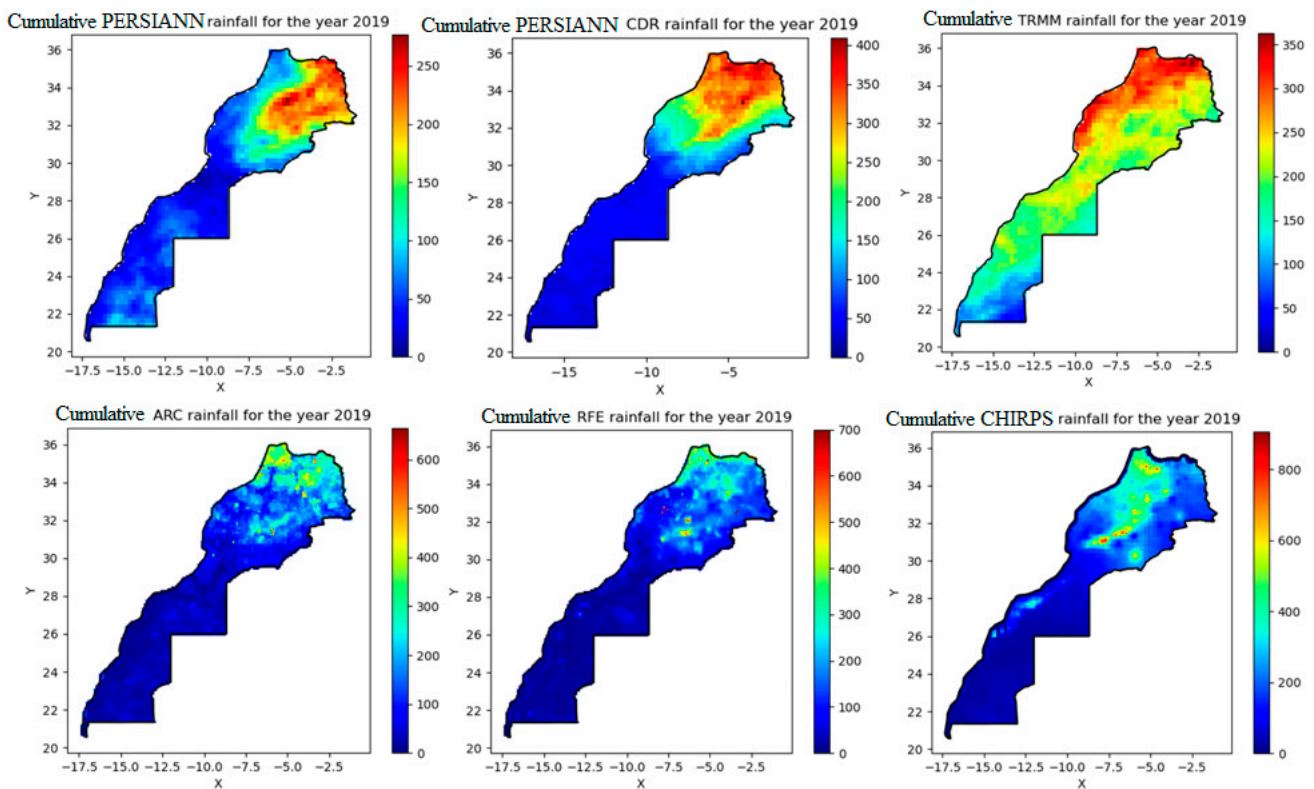
Figure 3. Simulated satellite-based cumulative rainfall for the year 2019.

3.2. Evaluation of Daily Precipitation

3.2.1. Evolution of Different Satellite Products of the Corresponding Pixel of Each Rain Gauge

Results of the temporal evolution of daily precipitation rates from the six weather stations in the Tensift basin and corresponding satellite pixels show that there is an annual variation in rainfall. The maximum daily precipitation per year varied from 25 mm in 2009 to 244 mm in 2014 at the Tachedert weather station. It can be observed that there is an underestimation of the satellite products for high altitudes and an overestimation for low altitudes, with an overestimation of ERA5, ARC2, and RFE2 (Figure 4). To have a clearer vision of the variations in precipitation rates, detailed analyses were performed on one of the wettest years (observations of significant spike around November 2014), and on the driest year (2019) (Figure S3). These showed a clear seasonal variation with two distinct periods: a wet period of 6 months from November to April (N–A) and a dry period that extended from June to September (J–S). These two periods are separated by the months of October and May, which are considered as transitional months. During the dry period, it is observed that TRMM overestimates the observations of weather stations, and this becomes more pronounced progressively towards lower altitudes (Grawa, Agdal, and Agafay) (Figure S3). This overestimation was more accentuated during the driest year (2019) and for a longer period (March–December). On the other hand, there was an underestimation of this product during the wet year (2014). During the wet period ERA, ARC2, and RFE2 products overestimated during heavy precipitation (mainly at medium and low altitudes (Asni, Grawa, Agdal, and Agafay) and underestimated during low rainfall (dry period), and especially during the driest year (2019) (Figure S3).
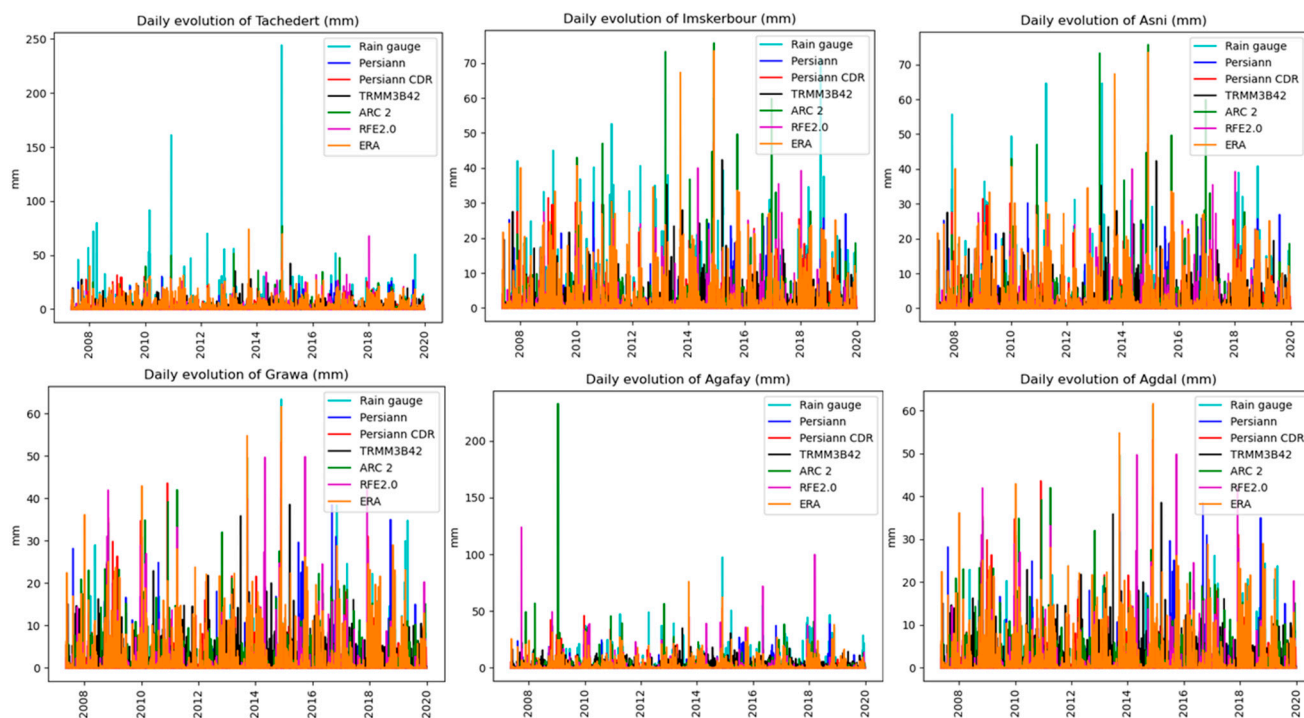
Figure 4. Temporal evolution of daily rainfall rates (mm) for each weather station and corresponding satellite pixels.

The observation made on the previous analyses (Figure S3) are reflected in Figure S4, in which TRMM sometimes overestimated during the driest year (2019), even when the period was wet; this is unlike the wet year (2014) where it only overestimated during the dry period (June to September). However, for the wettest year (2014), it is ERA5 and ARC2 that overestimated, followed by PERSIANN CDR. The latter products are increasingly close

to the weather stations in terms of response and intensity, especially when descending towards low altitudes (Asni, Grawa, and Agdal). On the other hand, for the year 2019, it was observed that it is not possible to identify systematic trends between these products. Indeed, whether for high altitudes (Tachedert) or low altitudes (Grawa, Agdal, and Agafay), significant differences in intensity between weather stations and satellite products are visible. In addition, variations and the overestimations of some products make it difficult to identify the best performing product during dry years.

3.2.2. Classical Metrics of Daily Satellite Precipitation and the Six Weather Station Observations in the Tensift Basin

Tachedert (2343 m)

The scatterplots of the relationship between the different satellite products (except for CHIRPS, because its precipitation data are mostly monthly) and the Tachedert weather station (2343 m) precipitation observations (Figure S6) have been presented with the aid of classical metrics (N, Nash; B, bias; RMSE, root-mean-square deviation; R, correlation coefficient; R^2, coefficient of determination) (Figure S6). The initial results show that Nash is positive for most of the products except for TRMM (-0.12). However, the positive Nash still presents very low and non-significant values (<0.7). For the bias, all products are negative, which is evidence of their underestimation at the Tachedert weather station, except for ERA, which overestimates the weather station data (0.15). RMSE records values that vary from 6.42 for PERSIANN CDR to 7.36 for TRMM. Regarding the correlation coefficient, PERSIANN CDR correlates the most with weather station observations with R = 0.4 followed by ERA (R = 0.35). On the other hand, TRMM is the least correlated product (R = -0.02). The latter observations are consistent with the coefficient of determination with R^2 = 0.161 for PERSIANN CDR and 0 for TRMM (Figure S6). From these results, it can be said that PERSIANN CDR has the best performance for high altitudes. This is confirmed by the Taylor diagrams (Figure 5), which shows that PERSIANN CDR has the highest correlation and the lowest RMSD, but the standard deviation is far from the observation (Red); in this case, the weather station of Tachedert detected precipitation of a very variable intensity (250 mm/d), hence the exorbitant value of the standard deviation.

Imskerbour (1404 m)

The scatterplots of the relationship between the different satellite products and the Imskerbour weather station (1404 m) (Figure S7) show that Nash is negative for half of the products and positive for ERA (0.28), RFE (0.12), PERSIANN CDR (0.03). For the bias, all products are negative, with the lowest value for PERSIANN CDR (-0.29), which is evidence of their underestimation at the Imskerbour weather station, except for ERA, which overestimates the weather station data (0.23). RMSE records values that vary from 6.53 for PERSIANN CDR to 7.36 for TRMM. Regarding the correlation coefficient, ERA correlates the most with weather station observations, with R = 0.62. On the other hand, TRMM is the least correlated product (R = -0.01). The latter observations are consistent for the coefficient of determination with R^2 = 0.388 for ERA and 0 for TRMM (Figure S7). From these results, it can be said that ERA has the best performance for medium altitudes. This is confirmed by the Taylor diagram (Figure 5) which shows that ERA has the highest correlation and the lowest RMSD with the closest value to the standard deviation of the observations at Imskerbour weather station.
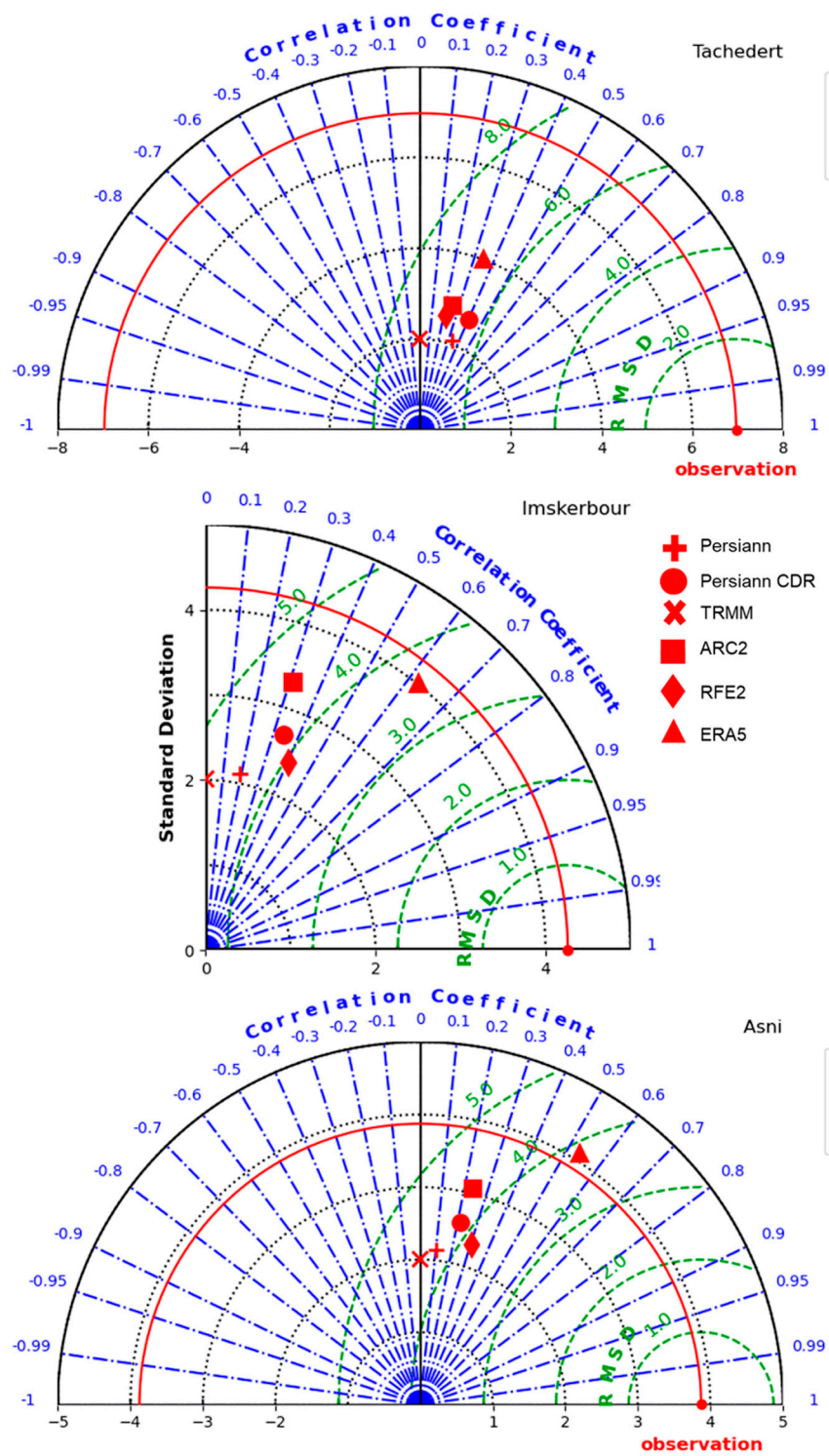
Figure 5. *Cont.*
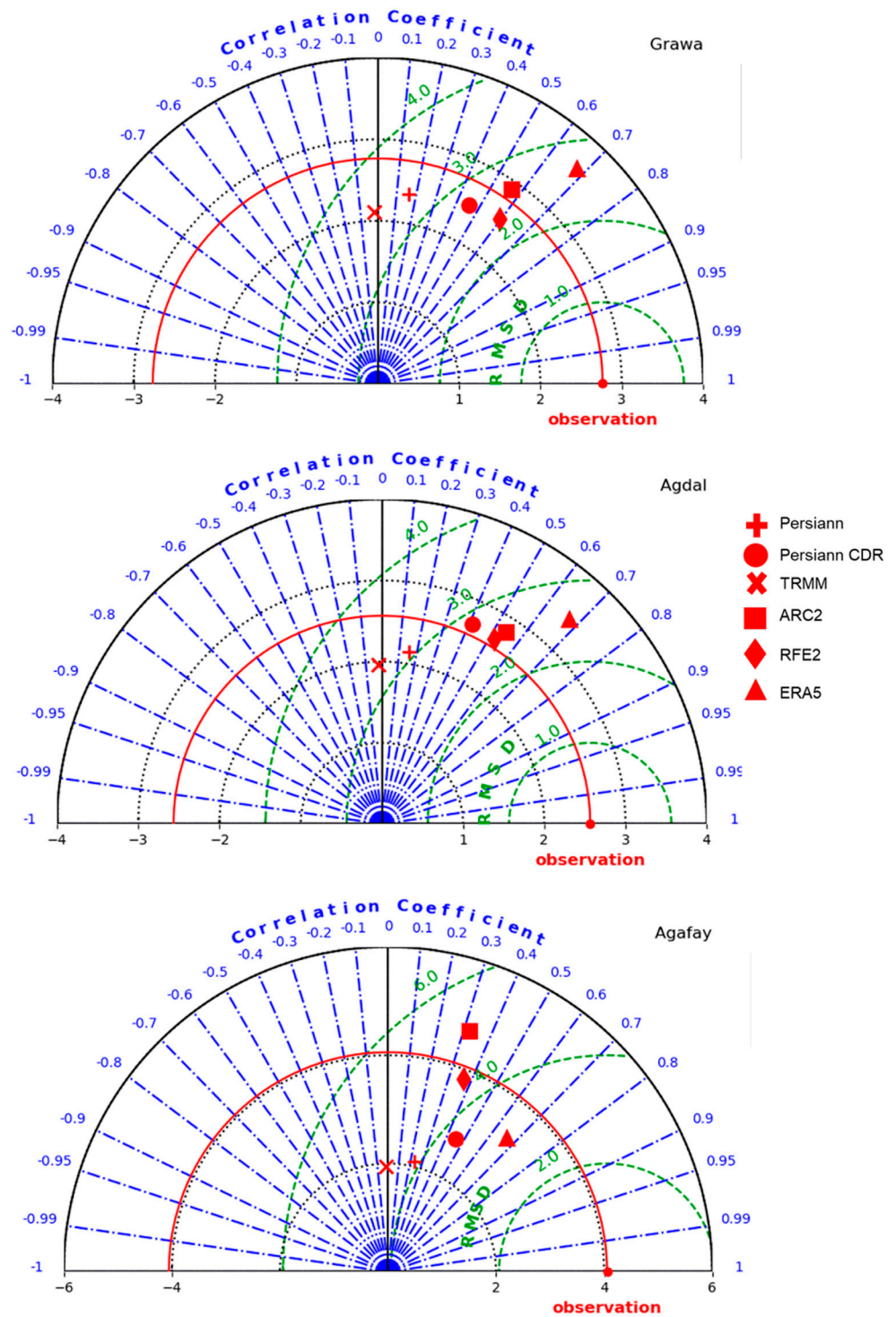
(**b**)

Figure 5. (**a**) Taylor diagrams of daily precipitation for Tachedert, Imskerbour, and Asni weather stations; (**b**) Taylor diagrams of daily precipitation for Grawa, Agdal, and Agafay weather stations.

Asni (1170 m)

From the scatterplots of the satellite products and the Asni weather station observations (Figure S8), it is seen that Nash is always negative except for ERA (0.14), which has a positive Nash value, greater than that recorded at Tachedert. The bias is, however, negative for all products except for ERA, which indicates an underestimation of this satellite product

at this weather station. However, it is lower in intensity than at Tachedert because these values are closer to 0. On the other hand, ERA overestimates the weather station data at Asni. RMSE shows values that vary from 3.58 for ERA followed by RFE with a value of 3.87 and then PERSIANN CDR (4.17), to 4.54 for ARC2. Therefore, the RMSE values recorded here are lower than at Tachedert, which confirms the hypothesis that the simulation improves as altitude reduces. The correlation coefficient and coefficient of determination show that ERA is the most correlated (R = 0.54, R^2 = 0.286), followed by RFE (R = 0.3, R^2 = 0.09); on the other hand, TRMM is the least correlated with R = −0.01 and R^2 = 0. Hence, it can be concluded that for medium altitudes, ERA is the best estimation product (Figure 6). This is confirmed by the Taylor diagram (Figure 5) which shows that ERA has the highest correlation and the lowest RMSD with the closest value to standard deviation of the observations.
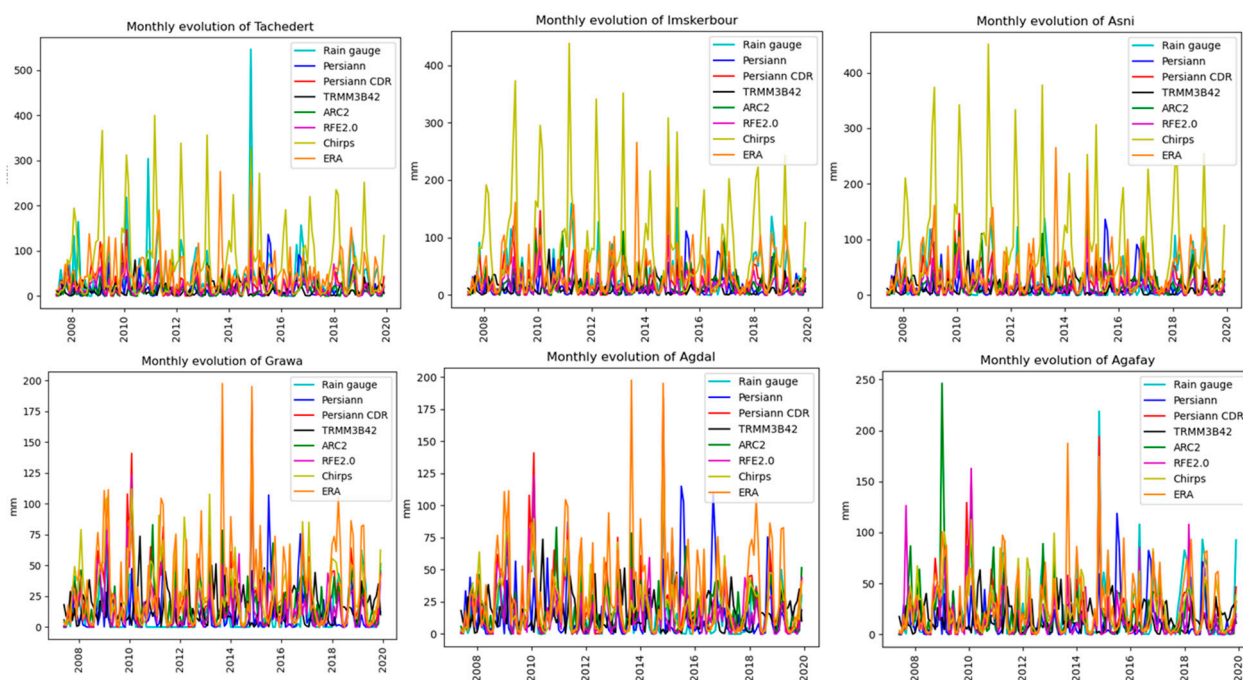
Figure 6. Temporal evolution of monthly rainfall rates (mm) for each weather station and corresponding satellite pixels.

Grawa (550 m)

The scatterplots of the relationship between weather station observations and satellite data at the Grawa weather station (Figure S9) show a Nash that is negative for half of the product and positive for RFE (0.25), ERA (0.21), and ARC (0.08). Concerning the bias, all the products overestimate the observation of the weather station of Grawa, except RFE (−0.01) and PERSIANN (−0.06). At this altitude, the lowest RMSE interval varies from 2.4 for RFE, followed by ERA (2.72), and then PERSIANN CDR (2.85), to 3.52 for TRMM. This justifies that the performance of the satellite and reanalysis products improves with the decreasing altitude. This is the case even for the values of correlation and the coefficient of determination which increase with the descending altitude. The R = 0.68 and R^2 = 0.463 for ERA is followed by RFE of R = 0.6, R^2 = 0.354. Hence, it is observed that for low altitudes, ERA5 and RFE2 are the best products for the daily estimation of rainfall rates in the Tensift basin. From the Taylor diagram (Figure 5), it can be concluded that RFE2 is the best because it has the closest value to standard deviation of the observations.

Agdal (489 m)

The scatterplots of the relationship between weather station observations and satellite data at the Agdal weather station (Figure S10) show negative Nash. Concerning the bias,

all the products overestimate the observation of the weather station of Grawa, except PERSIANN (-0.11). At this altitude, the lowest RMSE interval varies from 2.57 for RFE to 3.26 for TRMM. The correlation and coefficient of determination show that ERA is the most correlated (R = 0.67, R^2 = 0.455), followed by RFE (R = 0.52, R^2 = 0.268). Hence, it is observed that for low altitudes, ERA5 and RFE2 are the best products for daily estimations of rainfall rates in the Tensift basin. From the Taylor diagram (Figure 5), it can be concluded that RFE2 is the best because it has the closest value to the standard deviation of the observation.

Agafay (487 m)

From the scatterplots of the relationship between weather station observations and satellite data at the Agafay weather station (Figure S11), it is seen that Nash is always negative except for PERSIANN CDR (0.16) and ERA (0.41). Concerning the bias, all the products underestimate the observation of the weather station of Grawa, except ERA (0.08). At this altitude, the lowest RMSE interval varies from 3.09 for ERA to 4.54 for TRMM. The correlation and coefficient of determination show that ERA is the most correlated (R = 0.66, R^2 = 0.442), followed by PERSIANN CDR (R = 0.45, R^2 = 0.206). Hence, it is observed that for low altitudes, ERA5 and PERSIANN CDR are the best products for daily estimations of rainfall rates in the Tensift basin. From the Taylor diagram (Figure 5), it can be concluded that ERA5 is the best because it has a close value to the standard deviation of the observation.

3.3. Evaluation of Monthly Precipitation

3.3.1. Evolution of Different Satellite Products

In the context of the temporal evolution of monthly precipitation rates (mm), it is observed that the maximum precipitation varies from 546 mm in 2014 to 56 mm in 2019 for the weather station of Tachedert. Additionally, it is seen that the maximum of the monthly precipitation is more important in high-altitude areas than in low-altitude areas, with maximum intensities that vary from 500 mm in Tachedert (2343 m) to 200 mm in Grawa (550 m) and Agdal (489 m). In contrast to daily precipitation, the monthly estimates are closer to the Tachedert weather station observations, with the notable overestimation of CHIRPS product followed by ERA (Figure 6).

Analyses of one of the wettest years (2014) and the driest year (2019) (Figure S5) show that, for 2014, the observed seasonal variation that was observed earlier is maintained, with two distinct periods (one wet and the other dry) (Figure S5). Furthermore, there is an overestimation of TRMM during the dry period and an underestimation during the wet period. For the wet period (2014), there was an overestimation of CHIRPS, followed by ERA, and then PERSIANN CDR. In most cases, there is an overestimation of the estimated products, except for Tachedert, where most products are underestimated by the weather station data. Moving to the year 2019, the seasonal variations are not respected. Secondly, while the products have no trends, they have a little different response than the weather station records. In addition, CHIRPS and ERA overestimate at different altitudes, while TRMM is more prevailing than the year 2014 especially at low altitude. It can be concluded that daily and monthly satellite products estimate better at low altitude and in wet years (Figure S5).

3.3.2. Classical Metrics of Monthly Satellite Precipitation and the Six Weather Station Observations in the Tensift Basin

Tachedert (2343 mm)

From the scatterplots of the monthly satellite products with the Tachedert weather station observations (Figure S12), it is seen that Nash is negative for most of the products, except for PERSIANN CDR (0.3), ERA (0.27), and RFE (0.09). This is the case even for RMSE, with the lowest value for PERSIANN CDR (50.99). The bias shows that only CHIRPS and ERA overestimate the observations of Tachedert weather station. Regarding the correlation and coefficient of determination, ARC2 correlates the most with weather

station observations with R = 0.762 and R^2 = 0.581, followed by PERSIANN CDR (R = 0.667, R^2 = 0.446). From these results, it can be said that for monthly estimates, PERSIANN CDR is the closest to the high-altitude weather stations observations, because from the Taylor diagram (Figure 7), it can be observed that the PERSIANN CDR is closest to the standard deviation of Tachedert precipitation than ARC2. As can be noted, the values of correlation and coefficient of determination have improved from daily (Figure S6) to monthly (Figure S12) estimates, but in return, the errors (RMSE) have increased.

Imskerbour (1404 mm)

From the scatterplots of the monthly satellite products at the Imskerbour weather station (Figure S13), it is seen that PERSIANN CDR has the most significant NASH criterion (0.51). This is the case even for RMSE, with the lowest value for PERSIANN CDR (26.89). The bias shows that only CHIRPS and ERA overestimate the observations at the Imskerbour weather station. Regarding the correlation and coefficient of determination, PERSIANN CDR correlates the most with weather station observations, with R = 0.74 and R^2 = 0.545. From these results, it can be said that for monthly estimates, PERSIANN CDR is the closest to the medium-altitude weather stations observations. This is confirmed by the Taylor diagram (Figure 7), which shows that PERSIANN CDR has the highest correlation and the lowest RMSD with a value that is close to the standard deviation of the observations.

Asni (1170 m)

The scatterplots of the relationship between monthly weather station observations and satellite data at the Asni weather station (Figure S14) show that the most significant Nash criterion is attributed to PERSIANN CDR (0.18). This is the case even for RMSE, with the lowest value attributed to PERSIANN CDR (30.01). The bias shows that most of the products underestimate the Asni weather station observations. However, PERSIANN CDR is the product that overestimates the least (2.55) against ERA (18.09) and CHIRPS (51.72). Finally, it can be concluded that PERSIANN CDR is the most correlated (R = 0.544, R^2 = 0.296). From these results, it can be said that PERSIANN CDR is the best satellite product for estimating monthly precipitation at medium altitude. This is confirmed by the Taylor diagram (Figure 7), which shows that PERSIANN CDR has the highest correlation and the lowest RMSD, with the closest value to the standard deviation of the observations.

Grawa (550 m)

The results show that Nash is negative for all products (Figure S15). For the bias, all products are positive, which is evidence of their overestimation when compared with the Grawa weather station, except for PERSIANN which underestimates the weather station data (−1.42). The RMSE records values that are close between the different products, with the minimum attributed to RFE (19.96), followed by PERSIANN (20) and ARC2 (21.38), then PERSIANN CDR (24.26). Finally, it can be observed that PERSIANN CDR is the most correlated (R = 0.633, R^2 = 0.402), followed by ARC2 (R = 0.606, R^2 = 0.368); considering the different criteria, the best performance can be attributed to PERSIANN CDR and ARC2, for the estimation of monthly precipitation at low altitude. This is confirmed by the Taylor diagram (Figure 7), with a value that is close to the standard deviation of the observations of ARC2.

Agdal (489 m)

The results show that Nash is positive for most of the products except for ERA (−1.15), PERSIANN (−0.77), and TRMM (−0.71) (Figure S16). For the bias, all products are positive, which is evidence of their overestimation when compared with the Agdal weather station, except for PERSIANN, which underestimates the weather station data (−1.89). The RMSE records values of 14.64 for Chirps and 27.76 for ERA. Finally, it can be observed that PERSIANN CDR is the most correlated (R = 0.83, R^2 = 0.687), considering the different criteria; the best performance can be attributed to PERSIANN CDR and Chirps, for the

estimation of monthly precipitation at low altitude. This is confirmed by the Taylor diagram (Figure 7), with close values to the standard deviation of the observations to Chirps.

Agafay (487 m)

The results show that Nash is positive for most of the products with the highest value allocated to PERSIANN CDR (0.62) (Figure S17). For the bias, most of the products are negative, which is evidence of their underestimation when compared with the Agafay weather station with the lowest value for PERSIANN CDR (−1.9). The RMSE records values of 19.1 for PERSIANN CDR, and 37 for TRMM. Finally, it can be observed that PERSIANN CDR is the most correlated (R = 0.8, R^2 = 0.634). Considering the different criteria, the best performance can be attributed to PERSIANN CDR for the estimation of monthly precipitation at low altitude. The better performance of PERSIANN CDR is confirmed by Taylor diagram (Figure 7), with a value that is closest to the standard deviation of the observations of Agafay weather station.

(a)

Figure 7. *Cont.*

(b)
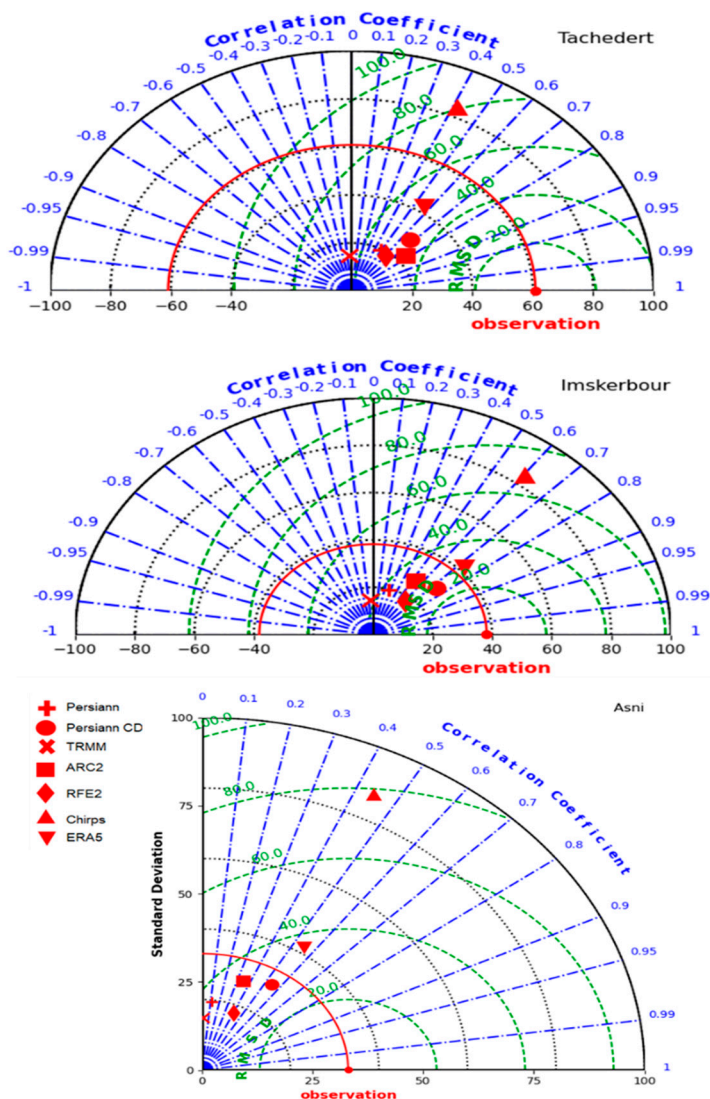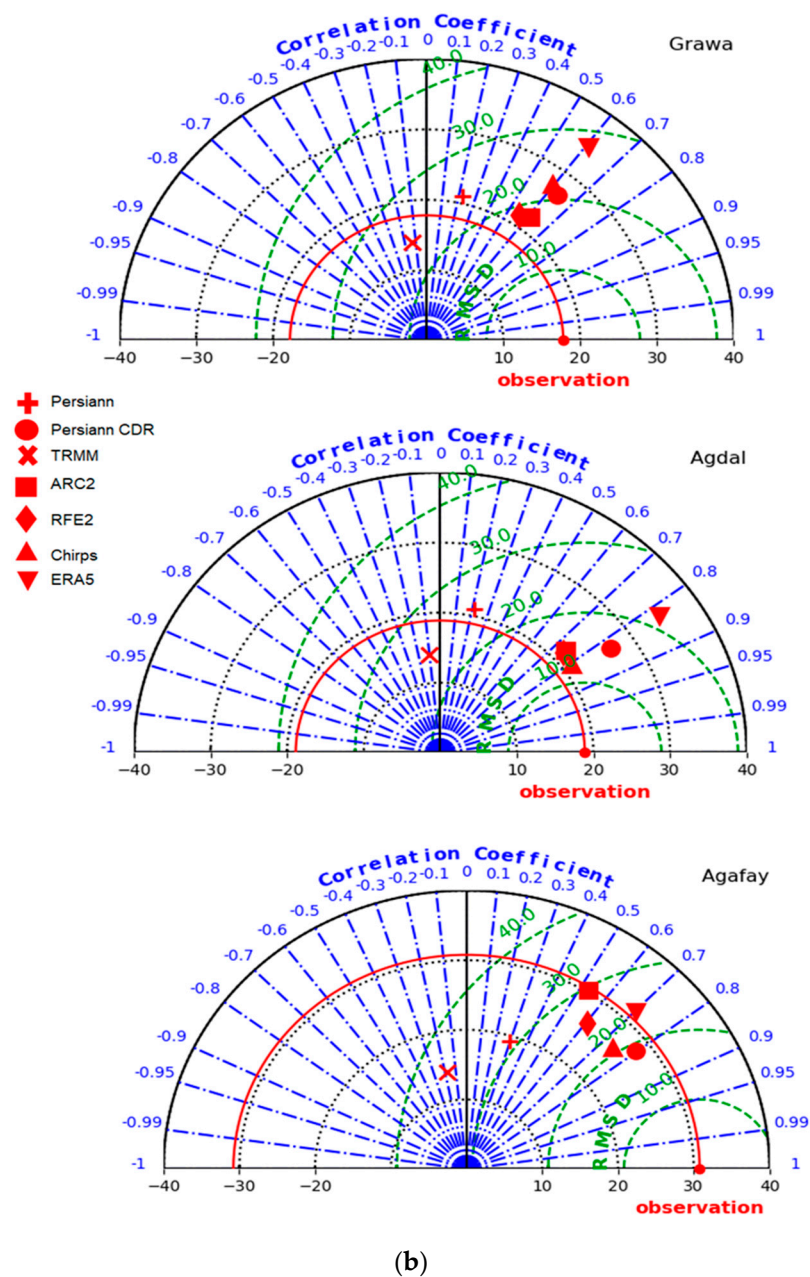
Figure 7. (**a**) Taylor diagram of monthly precipitation at Tachedert, Imskerbour, and Asni weather stations; (**b**) Taylor diagram of monthly precipitation at Grawa, Agdal, and Agafay weather stations.

3.4. Evaluation of Annual Rainfall

3.4.1. Evolution of Different Satellite Products

In the context of the temporal evolution of annual rainfall rates from the weather stations and corresponding satellite pixels (Figure 8), it is observed that the annual estimates are closer to the weather station observations at medium altitude (Imskerbour: 1404 m) (Asni: 1170 m), except for ERA and CHIRPS. For high altitudes (Tachedert: 2343 m), most of the satellite products underestimate, except for CHIRPS, and sometimes ERA. A previous study (El Orfi et al. [32]) has reported similar observations, noting that CHIRPS overestimates the rainfall data of weather stations during the rainy season, with positive bias values. For the low altitude (Grawa: 550 m, Agdal: 489 m, Agafay: 487 m) most of the satellite products overestimate the weather station data except for PERSIANN and sometimes TRMM and RFE. On the other hand, for Asni and Imskerbour, most of the

products are close to the weather stations observations, except for CHIRPS. Additionally, it is seen that at low altitude, especially for Grawa, TRMM begins to overestimate, because the amplitudes of overestimation during dry periods are more important than the amplitudes of underestimation during wet periods, which are not very frequent due to the arid climate of the Tensift region.
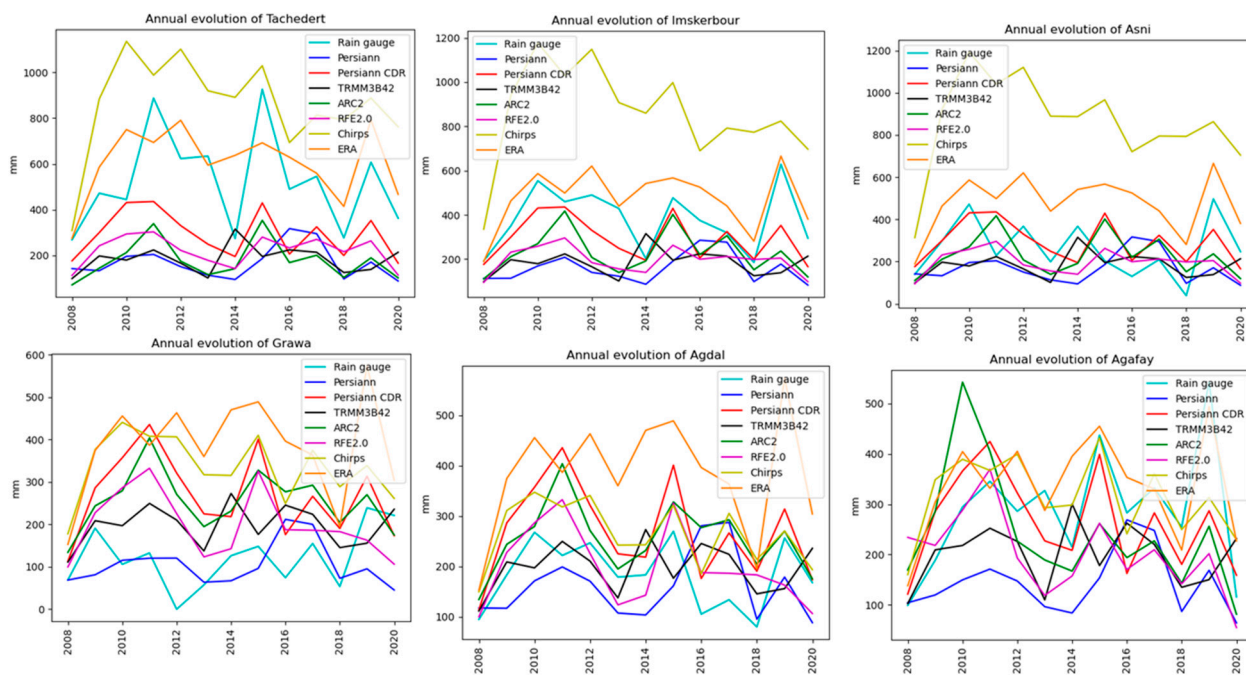
Figure 8. Temporal evolution of annual rainfall rates (mm) for each rain gauge and corresponding satellite pixels.

3.4.2. Classical Metrics of Annual Satellite Rainfall and the Six Weather Station Observations in the Tensift Basin

Tachedert (2343 m)

As can be observed in Figure S18, a negative Nash criterion for all the satellite products is recorded with PERSIANN CDR closest to 0 (−0.76); however, the reanalysis product ERA has a positive Nash of around 0.19 (Figure S18). For the bias, PERSIANN CDR underestimates the least (−232), and ERA overestimates the least (82). The latter product shows minimal error (RMSE = 185), followed by PERSIANN CDR (273), and then RFE (348). However, the correlation and coefficient of determination show that ARC2 is the most correlated (R = 0.864, R^2 = 0.748), followed by PERSIANN CDR (R = 0.777, R^2 = 0.605). From these results, it can be said that PERSIANN CDR is the best product for the estimation of annual products at high altitude. This is confirmed by the Taylor diagram (Figure 9), with the closest value to the standard deviation of the observations to PERSIANN CDR.

Imskerbour (1404 m)

As observed in Figure S19, a negative Nash criterion for all the satellite products is recorded except for PERSIANN CDR (0.16) and ERA (0.12). For the bias, PERSIANN CDR underestimates the least (−89), and ERA overestimates the least (96). PERSIANN CDR shows the minimal error (RMSE = 124). However, the correlation and coefficient of determination shows that ERA is the most correlated (R = 0.79, R^2 = 0.637), followed by PERSIANN CDR (R = 0.77, R^2 = 0.6). From these results, it can be said that PERSIANN CDR and ERA are the best estimators of annual products at medium altitude. This is confirmed by the Taylor diagram (Figure 9), with the closest value to the standard deviation of the observations attributed to ERA.
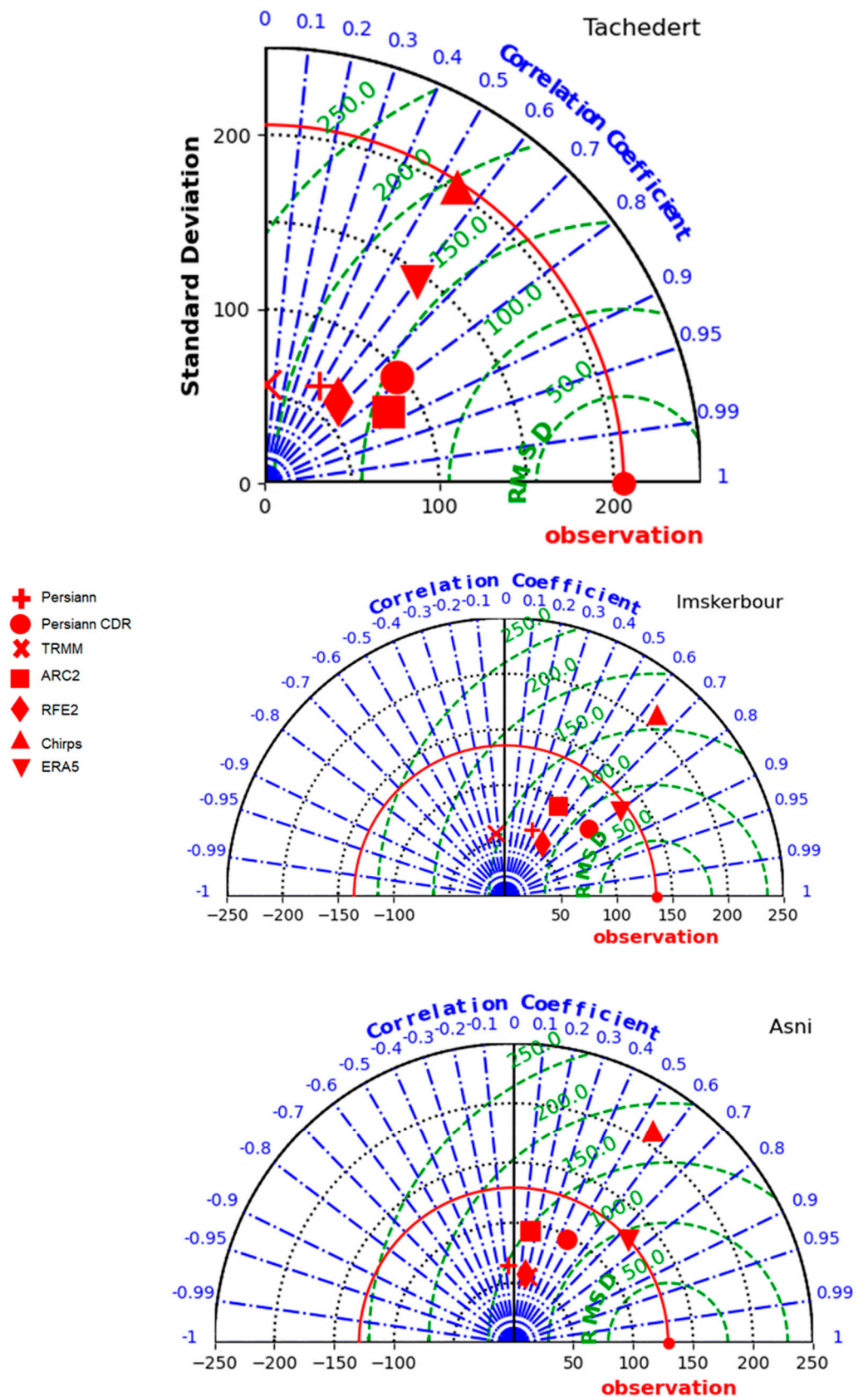
Figure 9. *Cont.*
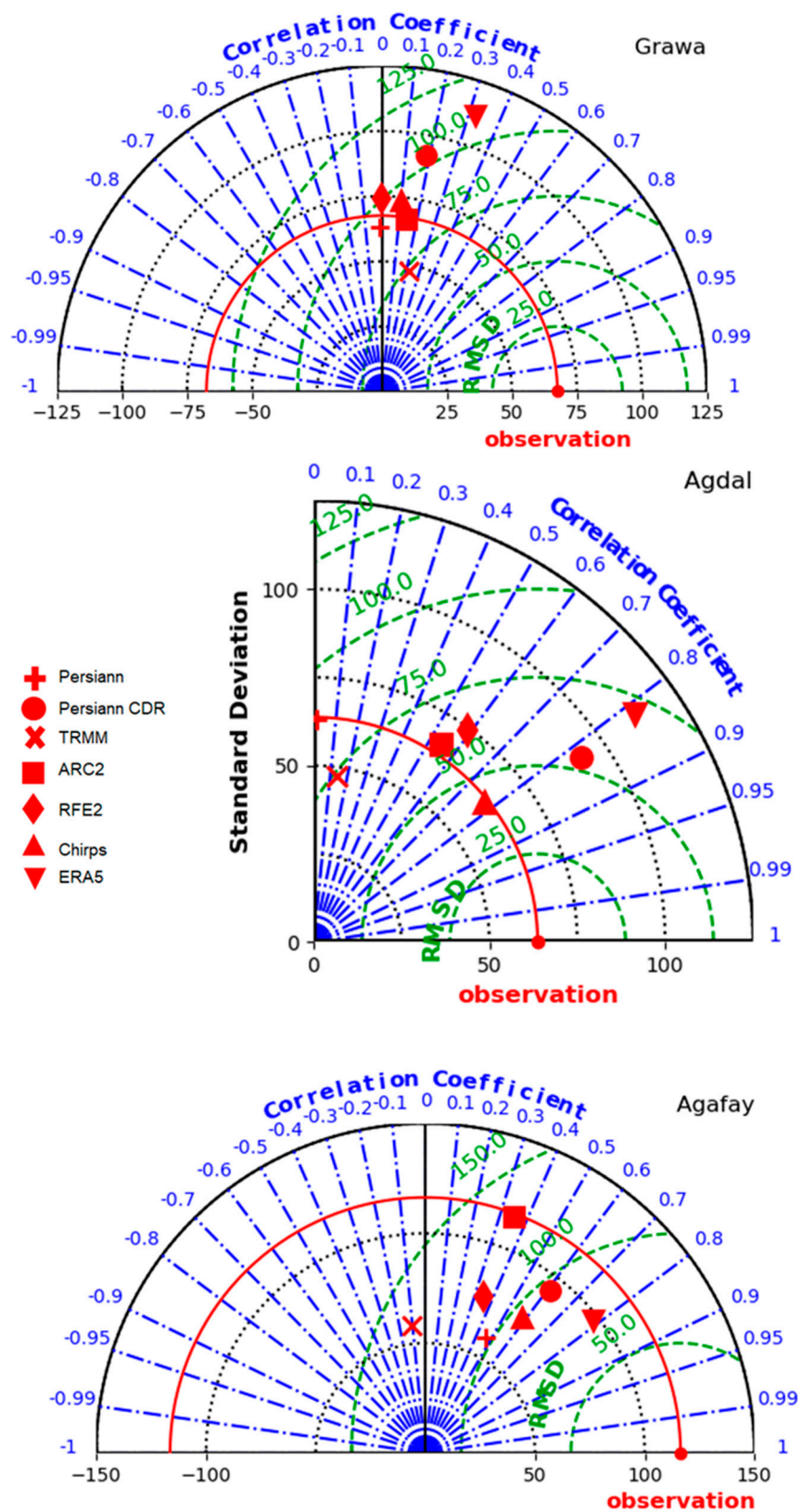
(**b**)

Figure 9. (**a**) Taylor diagram of the annual precipitation at Tachedert, Imskerbour, and Asni weather stations; (**b**) Taylor diagram of annual the precipitation at Grawa, Agdal, and Agafay weather stations.

Asni (1170 m)

Scatterplots of the relationship between annual weather station observations and satellite data at the Asni weather station (Figure S20) show that most of the products have a negative Nash, except for PERSIANN CDR (Nash = 0.06); this represents the minimum positive bias (B = 30.48). Similarly, for RMSE, PERSIANN CDR is the product that presents the least error, with RMSE = 125. ERA is the most correlated product in this case (R = 0.743, R^2 = 0.553), followed by CHIRPS (R = 0.55, r^2 = 0.303), then PERSIANN CDR (R = 0.453, r^2 = 0.206) (Figure S14). Considering all these criteria, it can be concluded that PERSIANN CDR is the best product for estimating annual precipitation at a medium altitude. From the Taylor diagram (Figure 9), it can be concluded that PERSIANN CDR is the best because it has a value close to the standard deviation of the observations.

Grawa (550 m)

The scatterplots of the relationship between annual weather station observations and satellite data at the Grawa weather station (Figure S21) show that all Nash estimates are negative, and therefore not significant. On the other hand, all the biases are positive implying that all the products overestimate the Grawa weather station observations except PERSIANN (B = −16.52). The minimum error is attributed to PERSIANN (RMSE = 90.92), followed by TRMM (RMSE = 106.16). For annual precipitation at low altitude, it can be observed that the correlation coefficients have decreased, unlike the monthly and daily coefficients. In fact, it varies from R = 0.32, R^2 = 0.103 for ERA, followed by R = 0.218, R^2 = 0.048 for TRMM, to R = −0.003, R^2 = 0 for RFE. From this, it can be concluded that for annual estimates at this low-altitude weather station, TRMM is functional, but not too efficient, because this performance was obtained only by the correction of the overestimation at low precipitation to the underestimation during heavy precipitation. This is confirmed by the Taylor diagram (Figure 9), which shows that TRMM has the highest correlation and the lowest RMSD with a low standard deviation.

Agdal (489 m)

The scatterplots of the relationship between annual weather station observations and satellite data at the Agdal weather station (Figure S22) show that all Nash estimates are negative, and therefore not significant. On the other hand, all the biases are positive, implying that all the products overestimate the Agdal weather station observations, except PERSIANN (B = −24). The minimum error is attributed to RFE (RMSE = 65), followed by TRMM (RMSE = 75). The correlation coefficient varies from R = 0.82, R^2 = 0.676 for PERSIANN CDR, to R = −0.01, R^2 = 0 for PERSIANN. From this, it can be concluded that for low altitudes and annual estimates, PERSIANN CDR and CHIRPS are the best products for annual precipitation at low altitude. This is confirmed by the Taylor diagram (Figure 9), which shows that the PERSIANN CDR has the highest correlation and CHIRPS has the lowest RMSD and the closest value to standard deviation of the observations of Agdal weather station.

Agafay (487 m)

The scatterplots of the relationship between annual weather station observations and satellite data at the Agafay weather station (Figure S23) show that most of the products have a negative Nash, and therefore are not significant, except ERA (0.44), PERSIANN CDR (0.3), and CHIRPS (0.27). On the other hand, most of the biases are negative, implying that most of the products underestimate the Agafay weather station observations with the lowest value being attributed to PERSIANN CDR. The minimum error is attributed to ERA (RMSE = 87), followed by PERSIANN CDR (RMSE = 98). The correlation coefficient varies from R = 0.78, R^2 = 0.612 for ERA, followed by R = 0.61, R^2 = 0.37 for PERSIANN CDR to R = −0.1, R^2 = 0 for TRMM. From this, it can be concluded that for low altitudes and annual estimates, PERSIANN CDR and ERA are the best products for annual precipitation at low altitude. This is confirmed by the Taylor diagram (Figure 9), which shows that ERA has the

highest correlation and the lowest RMSD followed by PERSIANN CDR with a value that is closest to the standard deviation of the observations of Agafay weather station.

3.5. Standardized Precipitation Index of Monthly Precipitation over the Tensift Basin

To determine the onset, duration, and magnitude of meteorological drought, the SPI time series is calculated based on the monthly precipitation resulting from the six weather stations for a period of 13 years (from May 2007 to December 2019). The temporal evolution of the SPI is based on the six weather stations in the Tensift basin. Figure 10 shows the initial results; the blue colors represent positive and wet outcomes, whereas the red colors represent the negative and dry periods. Below, we present the observations in each weather station.
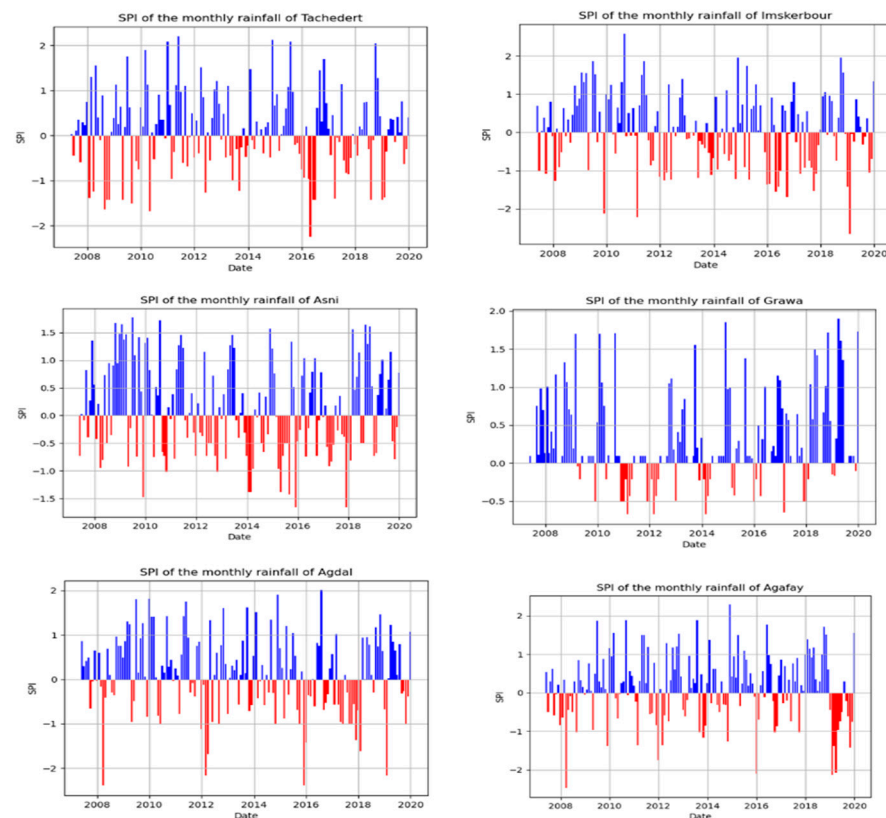
Figure 10. SPI of the monthly precipitation for the six weather stations in the Tensift basin.

3.5.1. Tachedert (2343 m)

The temporal evolution of the SPI based on the monthly precipitation at the Tachedert weather station shows that the lowest SPI (drought intensity: DI [2]) over the study period at Tachedert weather station is −2.25 (extremely dry), which corresponds to May 2016, and the highest is 2.19 (extremely wet), which corresponds to June 2011 (Figure 10). Based on statistical calculations, it was identified that Tachedert is part of the near-normal classification because the average SPI is equal to 0.087 (Table S3), and 73.68% of the data have an SPI included between −1 and 1. Drought severity (DS) is the cumulative absolute deficit of SPI over a drought event (or drought duration: DD), in which SPI is continuously below 0 with the lowest value <−1 [2]. It can be deduced from Figure 10 that the Tachedert weather station experienced six drought events (Table S4) over the study period (May 2007–December 2019), and 2016 was the driest year.

3.5.2. Imskerbour (1404 m)

The lowest SPI for the research period at the Imskerbour weather station is −2.66 (very dry), as shown by the temporal evolution of the SPI based on monthly precipitation at

the Imskerbour weather station (Figure 10), and the highest is 2.57 (extremely wet), which corresponds to February 2019. According to statistical calculations, Imskerbour belongs to the near-normal categorization because the average of SPI is 0.05 (Table S3) and 68.42% of the data have an SPI between −1 and 1. According to Figure 10 and Table S5, Imskerbour weather station saw ten drought occurrences over the study period, with 2019 being the driest.

3.5.3. Asni (1170 m)

The lowest SPI during the study period is −1.66 (very dry), which corresponds to December 2015 and 2017, and the highest is 1.77 (extremely wet), which corresponds to July 2009, according to the historical evolution of the SPI. Asni belongs to the near-normal categorization, because the average of SPI is 0.12 (Table S3) and 73.68% of the data have an SPI between −1 and 1. Based on Figure 10, Asni weather station had five drought occurrences (Table S6) over the research period, with 2015 being the driest year.

3.5.4. Grawa (550 m)

The temporal evolution of the SPI shows that the lowest SPI over the study period is −0.67 (near-normal) which corresponds to March 2011, 2012, and 2014, and the highest is 1.89 (severely wet), which corresponds to April 2019. Grawa is part of the near-normal classification because the average SPI is equal to 0.33 (Table S3), and 66.44% of the data have an SPI included between −1 and 1. It can be deduced from Figure 10 that Grawa weather station has not experienced any drought event over the study period (May 2007– December 2019).

3.5.5. Agdal (489 m)

Based on monthly precipitation data from the Agdal weather station, the lowest SPI for the research period is −2.39 (very dry), which corresponds to April 2008, and the highest is 2.01 (extremely wet), which corresponds to August 2016. According to statistical calculations, Agdal belongs to the near-normal categorization because its average SPI is 0.11 (Table S3) and 73.03% of the data have an SPI between −1 and 1. Agdal weather station saw ten drought occurrences throughout the research period (Table S7), with 2017 being the driest year, as shown in Figure 10.

3.5.6. Agafay (487 m)

The lowest SPI during the study period was −2.48 (very dry), which corresponded to April 2008, and the highest was 2.29 (extremely wet), which corresponded to December 2014. Agafay conforms to the near-normal classification, according to statistical calculations, because the average of SPI is 0.14 (Table S3) and 73.68% of the data have an SPI between −1 and 1. During the research period (May 2007–December 2019), the Agafay weather station had ten droughts (Table S8), as illustrated in Figure 10. As a result, 2017 may be considered Agafay's driest year during the study period.

4. Discussion

This study has evaluated the performance of several satellite rainfall products (PERSIANN, PERSIANN CDR, TRMM3B42 ARC2, RFE2, CHIRPS, and ERA5) and six precipitation station datasets in estimating precipitation in the Tensift basin. The Tensift basin was chosen because of its topographic complexity (the highest altitude in Morocco at Toubkal: 4167 m), its geographical position (central–western Morocco), and the scarcity of scientific scholarship and a comprehensive data platform from which the effects of climate variability on water resources can be studied. The bias, Nash–Sutcliffe efficiency, root-mean-square error, root-mean-square deviation, the standard deviation, and the coefficients of determination and correlation were computed using daily, monthly, and annual time steps to measure the capacity of the satellite data to recreate the observed rainfall. Taylor diagrams and scatterplots were generated in order to visualize the closeness between the seven satellite

products and the observed precipitation data. A second analysis was carried out on the monthly precipitation from the six weather stations based on the Standardized Precipitation Index in order to determine the onset, duration, and magnitude of the meteorological drought. The timeframe of the data used in the analysis spanned the period between the 13th of May 2007 and the 31st of December 2019. This timeframe was chosen based on the availability of data for the compared satellite products (Tables S1 and S2). Hence, the limitation of this work is mainly linked to the limited range of data (Start date: May 2007); however, this issue has been fixed by introducing SPI and Taylor diagrams. The key findings of this study show that the performance of these rainfall estimates is driven by topographic characteristics as well as the time steps and seasons.

Firstly, PERSIANN CDR products are valuable sources of information in the Tensift basin in the context of spatiotemporal drought monitoring, because these have the best performance at high altitudes (Tachedert: 2443 m) at different temporal resolutions (daily, monthly, and annual), at medium altitudes (Imskerbour: 1404 m, Asni: 1170 m) for monthly and annual precipitation, whereas for daily precipitation, the best performance is attributed to ERA, and for low altitudes (Agdal: 489 m, Agafay: 487 m) for monthly and annual precipitation. For daily precipitation, the best performance is attributed to RFE. This result will provide valuable information for water managers, irrigation planning, and drought management in the Tensift region. This is important because it simulates the relationship with weather station rainfall data more reliably than the other products. This finding is consistent with the findings of a study by Nguyen [18], which provides an evaluation of the performance of various satellite products such as PERSIANN (PERSIANN, PERSIANN CCS, and PERSIANN CDR) using the Climate Prediction Center (CPC) precipitation dataset as a baseline for comparison over the contiguous United States (CONUS) and at a global scale. The results of this study demonstrate a good performance of PERSIANN CDR compared with CPC, with a reasonable accuracy across different temporal and spatial scales. Indeed, this superiority can be explained, on one hand, by the bias adjustment of PERSIANN CDR on a monthly scale based on GPCP data, and on the other hand, by long-term historical records. This makes it suitable for investigating statistical trends in the historical extreme rainfall events and meteorological droughts as well as reconstructing historical stream flow observations.

This study has found that significant disparities exist between the various satellite products (Figures 1–3). For example, the average annual cumulative precipitation of the study period varies from 250 mm for TRMM to 1000 mm for CHIRPS. Similarly, a comparative review of global precipitation data presented by Sun [33] demonstrated a similar large difference between various satellite products, particularly in the mountains in North Africa. This difference can be explained by the restricted spatial coverage of surface stations, the satellite algorithms, and the data assimilation models.

Furthermore, this study has shown that TRMM underestimates rainfall during heavy rainfall and overestimates it during low rainfall. This finding is like those in previous studies by [19–22], who found that TRMM's annual observations in Morocco overestimate or underestimate weather station rainfall data during rainy and dry seasons, respectively. These articles also show that satellite data tend to overestimate rainfall in arid environments (see the bias of Grawa: Figures S9, S15 and S21), and underestimate it in sub-humid and high elevation areas (see the bias of Tachedert: Figures S6, S12 and S18). Similar observations were made by Gadouali [34] in Morocco. It has been argued that these flaws indicate that the new IMERG product's algorithms, particularly the research version, must be calibrated on a regular basis [34]. In addition, Milewski [20] observed that the bright band, ground clutter or attenuation of the reflectivity are causes of the poor performance of TRMM at high altitudes.

Again, Novella [24], argued that ARC2 outperforms TRMM at different spatiotemporal scales across Africa (Figure S24), with performance declining in the mountains, a similar observation found by this study. As can be observed (Figure S9), the coefficient of determination ($R^2 = 0.321$) of the relationship between ARC2 and the ground obser-

vations of Grawa is much higher than TRMM (R^2 = 0.001), and this coefficient declines with altitude, with R^2 = 0.06 for ARC2 and R^2 = 0 for TRMM at the Tachedert weather station (Figure S7). However, Gadouali [34] noted that ARC2 overestimates annual rainfall compared with RFE2, TRMM, and PERSIANN CDR over Morocco; an observation which is true even in this case of low altitude (Grawa) (Figure S21), but with a slight overestimation of PERSIANN CDR with bias = 146, followed by ARC2 = 133, then RFE2 = 78, and finally TRMM = 76. This slight discrepancy might be attributable to a comparison over all of Morocco [34], as opposed to this study, which focused just on the Tensift basin.

A study that compares PERSIANN, TRMM, and CMORPH over Africa by Serrat-Capdevila [21] reported that PERSIANN is the best product in the lowlands when compared with the other forms of data. However, its performance degrades as altitude increases. This was confirmed in the current investigation, as shown by the various scatterplots indicating that PERSIANN outperforms TRMM. The difficulties of predicting rainfall by TRMM in dry environments and in complex topographies were explained by the first TRMM comparison research in North Africa [20], in which they found that the desert's land surface characteristics influence upwelling microwave radiation (GMI). Additionally, it was observed that a high snow content and low rainfall in high altitudes are problematic for TRMM products; hence, the low correlation in this zone [20].

The comparison between the different altitudes driven by the location of the weather stations, as well as between dry and wet years, allowed us to deduce that the performance of the satellite products is better at low altitudes, due to changes in snow cover, winds, orography, and clouds, and during wet seasons. Similar investigations by [20–36] found that the lowest altitude had the highest degree of correlation and the lowest variation in bias, but the highest RMSE. This is probably due to the topographical effect, which reduces the measurement accuracy, or due to the presence of snow in high-altitude areas. Gadouali [34] has confirmed this by concluding that an altitude of less than 1000 m does not appear to impair the satellite product's performance in capturing the magnitude of rainfall events. On the other hand, they discovered that the lowest correlations occurred during dry years and in locations receiving less than 500 mm of rainfall per year [20].

Based on the monthly precipitation of the six weather stations at Tensift basin, spatiotemporal drought was investigated over the period May 2007 to December 2019. During this period, the Tensift basin experienced several drought episodes, which are summarized in Tables S4–S8. Hence, if all these drought events are merged without considering the weather stations, it can be deduced that the Tensift region has experienced 13 drought spells during the study period (Table S9). From Table S9, it can be concluded that the drought event from Marsh 2015 to February 2016 is the longest, with a DD of 12 months, and the drought of December 2018 to July 2019 was the most intense, with the highest drought severity (19.6) and the lowest SPI value (−2.66). Hence, it can be said that 2019 was the driest year for the Tensift basin.

On the other hand, discrepancies that show the scatterplots between satellite-based estimates of precipitation and ground-based measurements can be explained by the mismatch between the associated spatial resolutions; moreover, the observations of negative and low Nash, according to Serrat-Capdevila [21] and Gadouali [34], might be attributed to a paucity of ground observations in Africa and to the sensitivity of Nash to the presence of outliers at the daily step. Furthermore, [21] also demonstrated that bias correction does not improve the values obtained for this product in the Saharan desert and North Africa, indicating that most of the error in the region is correlation error. The latter is related to the difficulty of detecting rainfall correctly (Figure S25); as a result, bias adjustment was not used in this study.

There are studies that have employed similar techniques to those used in the current study. For example, [8] compared CMORPH, and MWCOMB satellite products and in situ data weather station data in southern Amazonia using bias, RMSE, coefficient of correlation, and coefficient of determination. However, to the best of our knowledge, no studies have been published in the scientific scholarship that quantify these criteria or

analyze seven satellite products over the Tensift basin at three different altitudes and time steps. It has been argued that, because of the scarcity of monitoring stations required for statistical comparison, research in arid environments, particularly in the MENA region, is limited [32,35,36]. Hence, the results of this study could provide valuable information by proving that PERSIANN CDR is the most reliable satellite product in the Tensift region. From now on, all water and climate researchers, as well as water managers in the Tensift region, Morocco, or even all African countries with similar climate and topography, will have access to a satellite product with a long history (since 1983), a high spatial and temporal resolution ($0.25°$, 1 day), and good performance at high, medium, and low altitudes, and at various temporal scales (daily, monthly, and annual). This can be used, firstly, for improving our understanding of the effects of climate variability on water resources in the Tensift basin; secondly, to study the impact of climate change, because historical data from rain gauges in this region do not allow that; and finally, to predict future rainfall based on a powerful satellite product to see the impact of global warming in the future for the better management of extreme phenomena in the Tensift region.

5. Conclusions

In conclusion, the comparison of the satellite products and weather station data shows significant disparities between the different products (CHIRPS = 2000 mm/TRMM = 400 mm). The disparities are mainly due to data processing issues, namely, the use of different algorithms and databases (GEO/LEO). This suggests that further work should be carried out to improve their determination as a function of altitude and weather conditions as well as the introduction of more weather stations across Morocco in general and the Tensift basin. However, based on time and altitudes, there are only two cases for which the best performance was not attributed to PERSIANN CDR. The first case was for daily rainfall at medium altitude, where the best performance was attributed to ERA5, and the second case was attributed to RFE for daily rainfall at low altitude. Hence, it can be deduced that PERSIANN CDR is the best satellite product to be used to study the effects of climate change in the Tensift basin. This is based on its ability to simulate rainfall rates over a wide spatial and temporal range and with a long history (since 1983). This aspect further proves the originality of this study. In addition, during the processing of these products, other constraints were encountered that influenced the results, and thus, the interpretation. Indeed, the overestimation of the TRMM product during heavy precipitation and underestimation during low precipitation induced a correction of overestimated intensities to the underestimated, and consequently, the improvements in the statistical criteria for annual precipitation at Grawa weather station. This makes the interpretation of the comparison of the annual rates difficult. It is also worth mentioning that the performance of the estimates increases towards lower altitudes, due to changes in snow cover, winds, orography, and clouds. The comparison between the different altitudes and between dry and wet years allowed us to deduce that the performance of the satellite products is better at low altitudes and during wet seasons. Low and negative Nash values may be due to insufficient weather stations in the study area, because most of the satellite algorithms are based on a calibration of the output products to the ground observations. This highlights the need to develop more weather stations in the Tensift region. Moreover, some discrepancies between satellite-based estimates of precipitation and ground-based measurements can be explained by the mismatch between the associated spatial resolutions. This study has been limited to analyzing the effects of climate change due the limited historical data, because the weather stations are recent (May 2007), although this issue has been addressed by analyzing climate variability based in SPI, Taylor diagrams, and some statistical criteria (Nash, RMSE, R, and R^2). Lastly, this study improves knowledge on the effects of climate change on water resources in the Tensift region. Going forward, it would be important to carry out studies that estimate possible future projections as well as the role of temperature-based satellite products and weather station data in the same basin. Studies with more elaborate data from more weather stations, more satellite products as well as a longer historical time

series data for SPI analysis will be necessary to further validate these results and enhance climate predictions. These results are original because the approach of comparing these seven satellite products with six weather-station-based datasets has never been performed in Morocco, neither in the Tensift basin.

References

1. The Intergovernmental Panel on Climate Change (IPCC), AR6, Synthesis Report: Climate Change 2022. Available online: https://www.ipcc.ch/report/sixth-assessment-report-cycle/ (accessed on 20 October 2021).
2. Habito, N.A.; Morabbi, D.; Ouazar, A.; Bouziane, M.D.; Hasnaoui, H. CHIRPS precipitation open data for drought monitoring: Application to the Tensift basin, Morocco. *J. Appl. Remote Sens.* **2020**, *14*, 034526. [CrossRef]
3. Schilling, J.; Freier, K.P.; Hertig, E.; Scheffran, J. Climate change, vulnerability, and adaptation in North Africa with focus on Morocco. *Agric. Ecosyst. Environ.* **2021**, *156*, 12–26. [CrossRef]
4. Driouech, F. Distribution des Précipitations Hivernales sur le Maroc Dans le Cadre d'un Changement Climatique: Descent échelle et Incertitudes. Ph.D. Thesis, Institut National Polytechnique de Toulouse, Toulouse, France, 2010. Available online: https://oatao.univ-toulouse.fr/7237/ (accessed on 15 October 2021).
5. Alves de Souza, B.; da Silva Rocha Paz, I.; Ichiba, A.; Willinger, B.; Gires, A.; Carlos Cesar Amorim, J.; de Miranda Reis, M.; Tisserand, B.; Tchiguirinskaia, I.; Schertzer, D. Multi-hydro hydrological modelling of a complex peri-urban catchment with storage. *Hydrol. Sci. J.* **2018**, *63*, 1619–1635. [CrossRef]
6. Sauvageot, H. Mesures Hydrologiques. Laboratoire d'Aérologie Université Paul Sabatier, Toulouse. La Houille Blanche, 1983, N° 5/6- 330-338. Available online: https://www.univ-tlse3.fr/laboratoire-d-aerologie-1 (accessed on 20 October 2021).
7. Roca, R.P.; Chambon, I.; Jobard, P.E.; Kirstetter, M.; Gosset, J.; Berges, C. Comparing Satellite and Surface Rainfall Products over West Africa at Meteorologically Relevant Scales during the AMMA Campaign Using Error Estimates. *J. Appl. Meteorol. Climatol.* **2009**, *49*, 715–731. [CrossRef]
8. Delahaye, F. Analyse Comparative des Différents Produits Satellitaires D'estimation des Précipitations en Amazonie Brésilienne. 2003. Available online: https://tel.archives-ouvertes.fr/tel-00824885 (accessed on 15 September 2021).
9. Giorgio, F.C.; Jones, G.; Asrar, R. L'expérience CORDEX: Répondre aux Besoins D'information Climatologique à L'échelle Régionale. *Bulletin De L'Omm* **2009**, *58*, 175. Available online: https://public.wmo.int/fr/bulletin/l%E2%80%99exp%C3%A9rience-cordex-r%C3%A9pondre-aux-besoins-d%E2%80%99information-climatologique-%C3%A0-l%E2%80%99%C3%A9chelle-r%C3%A9gionale (accessed on 9 June 2021).
10. Moucha, A.; Hanich, L.; Tramblay, Y.; Saaidi, A.; Gascoin, S.; Martin, E.; Le Page, M.; Bouras, E.; Szczypta, C.; Jarlan, L. Present and Future High-Resolution Climate Forcings over Semiarid Catchments: Case of the Tensift (Morocco). *Atmosphere* **2021**, *12*, 370. [CrossRef]
11. TREMA. Le Basin Du Versant Du Tensift. 2020. Available online: https://www.lmi-trema.ma/contexte/le-bassin-versant-du%20tensift/ (accessed on 14 July 2021).
12. Er-Raki, S.; Amazirh, A.; Ayyoub, A.; Khabba, S.; Merlin, O.; Ezzahar, J.; Chehbouni, A. Integrating Thermal Surface Temperature into Penman Monteith Model for estimating evapotranspiration and crop water stress of orange orchard in semi-arid region. *Acta Hortic.* **2018**, *1197*, 89–96. [CrossRef]
13. El Khalki, E.M.; Tramblay, Y.; El Mehdi Saidi, M.; Bouvier, C.; Hanich, L.; Benrhanem, M.; Alaouri, M. Comparison of modeling approaches for flood forecasting in the High Atlas Mountains of Morocco. *Arab. J. Geosci.* **2018**, *11*, 1–15. [CrossRef]

14. Baba, M.W.; Gascoin, S.; Jarlan, L.; Simonneaux, V.; Hanich, L. Variations of the Snow Water Equivalent in the Ourika Catchment (Morocco) over 2000–2018 Using Downscaled MERRA-2 Data. *Water* **2018**, *10*, 1120. [CrossRef]

15. The Center for Hydrometeorology and Remote Sensing (CHRS). CHRS Irain. Available online: http://irain.eng.uci.edu/ (accessed on 12 July 2021).

16. The Center for Hydrometeorology and Remote Sensing (CHRS). Date Portal. Available online: http://chrsdata.eng.uci.edu/ (accessed on 12 July 2021).

17. The Center for Hydrometeorology and Remote Sensing (CHRS). CHRS Rain Sphere. Available online: http://rainsphere.eng.uci.edu/ (accessed on 12 July 2021).

18. Nguyen, P.; Ombadi, M.; Sorooshian, S.; Hsu, K.; AghaKouchak, A.; Braithwaite, D.; Ashouri, H.; Thorstensen, A.R. The Persiann family of global satellite precipitation data: A review and evaluation of products. *Hydrol. Earth Syst. Sci.* **2018**, *22*, 5801–5816. [CrossRef]

19. Hadria, R.; Boudhar, A.; Ouatiki, H.; Lebrini, Y.; Elmansouri, L.; Gadouali, F.; Lionboui, H.; Benabdelouahab, T. Combining Use of TRMM and Ground Observations of Annual Precipitations for Meteorological Drought Trends Monitoring in Morocco. *Am. J. Remote Sens.* **2019**, *7*, 25–34. [CrossRef]

20. Milewski, A.; Elkadiri, R. Durham, M. Assessment and Comparison of TMPA Satellite Precipitation. Products in Varying Climatic and Topographic Regimes in Morocco. *Remote Sens.* **2015**, *7*, 5697–5717. [CrossRef]

21. Serrat-Capdevila, A.; Merino, M.; Valdes, J.B.; Durcik, M. Evaluation of the Performance of Three Satellite Precipitation Products over Africa. *Remote Sens.* **2016**, *8*, 836. [CrossRef]

22. Ouatiki, H.; Boudhar, A.; Tramblay, Y.; Jarlan, L.; Benabdelouhab, T.; Hanich, L.; El Meslouhi, M.R.; Chehbouni, A. Evaluation of TRMM 3B42 V7 Rainfall Product over the Oum Er Rbia Watershed in Morocco. *Climate* **2017**, *5*, 1. [CrossRef]

23. NASA. Earth Data. Available online: https://earthdata.nasa.gov/ (accessed on 12 July 2021).

24. Novella, N.S.; Thiaw, W.M. African Rainfall Climatology Version 2 for Famine Early Warning systems. *J. Appl. Meteorol. Climatol.* **2012**, *52*, 588–606. [CrossRef]

25. International Research Institute for Climate and Society. Building Sustainable Climate Solutions for Food Security. Available online: https://iri.columbia.edu/ (accessed on 12 July 2021).

26. NOAA. CPC GIS Data. Available online: https://www.cpc.ncep.noaa.gov/products/GIS/GIS_DATA/ (accessed on 12 July 2021).

27. Funk, C.; Peterson, P.; Landsfeld, M.; Pedreros, D.; Verdin, J.; Shukla, S.; Husak, G.; Rowland, J.; Harrison, L.; Hoell, A.; et al. The climate hazards infrared precipitation with stations—A new environmental record for monitoring extremes. *Sci. Data* **2015**, *2*, 1–21. [CrossRef] [PubMed]

28. USGS. CHIRPS Data. Available online: https://edcintl.cr.usgs.gov/downloads/sciweb1/shared/fews/web/global/monthly/chirps/final/downloa%20ds/monthly/ (accessed on 12 July 2021).

29. Gleixner, S.; Demissie, T.; Tefera Diro, G. Did ERA5 Improve Temperature and Precipitation Reanalysis over East Africa? *Atmosphere* **2020**, *11*, 996. [CrossRef]

30. Jiang, Q.; Li, W.; Fan, Z.; He, X.; Sun, W.; Chen, S.; Wen, J.; Gao, J.; Wang, J. Evaluation of the ERA5 reanalysis precipitation dataset over Chinese Mainland. *J. Hydrol.* **2021**, *595*, 125660. [CrossRef]

31. Climate Change Service. ECMWF. Available online: https://cds.climate.copernicus.eu/%23!/home (accessed on 12 July 2021).

32. El Orfi, T.; El Ghachi, M.; Lebaut, S. Comparaison des données de précipitation satellitaires avec les données mesurées dans le bassin versant de l'Oued Oum Er Rbia en amont du barrage Ahmed El Hansali (Maroc). In *XXXIIIème Colloque de l'Association Internationale de Climatologie: Changement Climatique Et Territoires*; Loterr: Rennes, France, 2020; pp. 271–276.

33. Sun, Q.; Miao, C.; Duan, C.; Ashouri, H.; Sorooshian, S.; Hsu, K.L. A review of global precipitation data sets: Data sources, estimation, and intercomparisons. *Rev. Geophys.* **2018**, *56*, 79–107. [CrossRef]

34. Gadouali, F.; Messouli, M. Evaluation of multiple satellite-derived rainfall products over Morocco. *Int. J. Hydrol. Sci. Technol.* **2020**, *10*, 72–89. [CrossRef]

35. Al Bitar, A.; Najem, L.; Jarlan, M.; Zribi, G.; Faour, G. Precipitation, and soil moisture datasets show severe droughts in the MENA region. *Res. Sq.* **2020**. [CrossRef]

36. Youssef, H. Modélisation hydrologique du bassin versant de l'oued Rheraya et sa contribution à la recharge de la nappe du Haouz (bassin du Tensift, Maroc). Hydrologie. Ph.D. Thesis, Université Paul Sabatier—Toulouse III, Toulouse, France, 2018.